FINITE ELEMENT MODELLING OF DEFECTIVE CARBON NANOTUBE REINFORCED POLYMER COMPOSITES

A THESIS SUBMITTED TO
THE BOARD OF CAMPUS GRADUATE PROGRAMS
OF MIDDLE EAST TECHNICAL UNIVERSITY
NORTHERN CYPRUS CAMPUS

BY

COŞKUN KAĞAN ÖZEL

IN PARTIAL FULLFILLMENT OF THE REQUIREMENTS
FOR
THE DEGREE OF MASTER OF SCIENCE
IN
SUSTAINABLE ENVIRONMENT AND ENERGY SYSTEMS

AUGUST 2019

Approval of the Board of Graduate Programs

Prof. Dr. Gürkan Karakaş
Chairperson

I certify that this thesis satisfies all the requirements as a thesis for the degree of Master of Science.

Assist. Prof. Dr. Ceren İnce Derogar
Program Coordinator

This is to certify that we have read this thesis and that in our opinion it is fully adequate, in scope and quality, as a thesis for the degree of Master of Science.

Assoc. Prof. Dr. Volkan Esat
Supervisor

Examining Committee Members

Assoc. Prof. Dr. Volkan Esat	Mechanical Engineering Prog. METU NCC	
Assist. Prof. Dr. Ceren İnce Derogar	Civil Engineering Prog. METU NCC	
Assist. Prof. Dr. Süleyman Aşır	Materials Science and Nanotechnology Engineering Dept. Near East U	

ETHICAL DECLARATION

I hereby declare that all information in this document has been obtained and presented in accordance with academic rules and ethical conduct. I also declare that, as required by these rules and conduct, I have fully cited and referenced all material and results that are not original to this work.

Name, Last Name: Coşkun Kağan, Özel

Signature :

ABSTRACT

FINITE ELEMENT MODELLING OF DEFECTIVE CARBON NANOTUBE REINFORCED POLYMER COMPOSITES

Özel, Coşkun Kağan

M.S., Sustainable Environment and Energy Systems Program

Supervisor: Assoc. Prof. Dr. Volkan Esat

August 2019, 79 Pages

Carbon nanotubes (CNTs) attract significant attention being one of the superior engineering materials that possess exceptional material properties. One of the uses of carbon nanotubes is as reinforcements in a polymer matrix to form Carbon Nanotube Reinforced Polymer (CNTRP) composites. CNTRPs are lightweight structures with enhanced mechanical properties due to CNT addition. It is well known that CNTs do not usually exist in perfect structural form. They possess defects such as vacancies or Stone-Wales (SW) defects. These defects have the potential to significantly affect the mechanical properties and thus the mechanical response of the CNT under loading conditions. This study aims to model various defective CNTs with different geometric and structural properties in order to investigate essential mechanical properties more realistically using nano-scale equivalent continuum modelling. Then, CNTRP composites are modelled that contain CNTs with defects. The developed CNTRP composite finite element models are then utilised to bring a more realistic insight into their properties and responses under mechanical load. First part of the study focuses on the

investigation of single-walled carbon nanotubes (SWNTs) with Stone-Wales, mono-vacancy, di-vacancy, and combination of these defects. Zigzag and armchair configurations are considered with different diameters for the simulations. Results clearly show that defects may have significant effects on mechanical properties in the form of Young's modulus, shear modulus and Poisson's ratio. The second part of the thesis focuses on modelling of defective CNTRPs. The study on CNTRPs are carried out for 5% volume fraction of SWNTs. CNTRPs are modelled via continuum approaches. Results indicate that presence of defects can affect Young's modulus and Poisson's ratio adversely depending on diameter and chirality of tubes.

Keywords: single-walled carbon nanotube, Stone-Wales defect, mono-vacancy defect, di-vacancy defect, carbon nanotube reinforced composite, carbon nanotube reinforced epoxy composite, equivalent continuum modelling

ÖZ

KUSURLU KARBON NANOTÜP TAKVİYELİ POLİMER KOMPOZİTLERIN SONLU ELEMANLAR YÖNTEMİYLE MODELLENMESİ

Özel, Coşkun Kağan

Yüksek Lisans, Sürdürülebilir Çevre ve Enerji Sistemleri Programı
Tez Yöneticisi: Doç. Dr. Volkan Esat

Ağustos 2019, 79 sayfa

Karbon nanotüpler (KNT) olağanüstü malzeme özellikleriyle üstün mühendislik malzemelerinden sayılmakta ve ilgi çekmektedirler. Karbon nanotüplerin kullanım alanlarından biri Karbon Nanotüp Takviyeli Polimer (KNTTP) kompozit elde etmek amacıyla takviye elemanı olarak işlev görmeleridir. KNTTP'ler özellikleri KNT takviyesinden ötürü iyileştirilmiş hafif yapılardır. Karbon nanotüplerin gerçek hayatta genelde mükemmel bir yapıya sahip olmadıkları; boş köşe veya Stone-Wales kusurları gibi kusurları olduğu bilinmektedir. Bu kusurların karbon nanotüplerin mekanik malzeme özelliklerini ve dolayısıyla yükleme altında davranışlarını etkileme potansiyeli bulunmaktadır. Bu çalışma çeşitli geometrik ve yapısal özelliği haiz kusurlu KNT'lerin, temel mekanik özelliklerinin incelenebilmesi için nano boyutta eşdeğer sürekli ortamlar modellemesiyle oluşturulmasını hedeflemektedir. Sonrasında kusurlu KNT ile takviye edilmiş KNTTP kompozit modelleri oluşturulmuştur. Oluşturulan KNTTP kompozit sonlu elemanlar modelleri malzeme özelliklerinin ve yükleme altında davranışlarının daha gerçekçi

bir şekilde incelenebilmesi için kullanılmıştır. Çalışmanın ilk parçası içerisinde Stone-Wales, tek boşluk, çift boşluk kusurları ve bunların kombinasyonlarının bulunduğu tek duvarlı karbon nanotüp modellerinin incelenmesine odaklanılmıştır. Simülasyonlarda zigzag ve armchair şekillenimlerine sahip farklı çaplara sahip tüpler kullanılmıştır. Sonuçlarda görülebileceği üzere kusurların tüplerin mekanik özelliklerinden olan Young (elastisite) modülü, kesme modülü ve Poisson oranına etkileri önemli derecelere çıkabilmektedir. Tezin ikinci kısmında ise kusurlu KNTTP kompozitler modellenmiştir. Çalışma %5 KNT hacim oranına sahip polimer kompozitleri için yapılmıştır. Elde edilen sonuçlara göre kusurların eklenmesi KNTTPlerin Young modülü ve Poisson oranına çap ve şekillenim tipine bağlı olarak farklı oranlarda olumsuz etkilediği gözlenmiştir.

Anahtar kelimeler: tek duvarlı karbon nanotüp, Stone-Wales kusuru, tek boşluk kusuru, çift boşluk kusuru, Karbon Nanotüp Takviyeli Polimer kompozit, eşdeğer sürekli ortamlar modellemesi

DEDICATION

To my beloved

Parents, brother and all my family.

ACKNOWLEDGEMENTS

I would like to express my deepest respect and gratitude to my thesis adviser, Assoc. Prof. Dr. Volkan Esat for his valuable and continuous advice, guidance and support during this period to make this work possible.

Also, I would like to thank all my committee members, Assist. Prof. Dr. Ceren İnce Derogar, and Assist. Prof. Dr. Süleyman Aşır, for their time, comments, considerations during the whole reviewing / refereeing process.

I would like to thank to METU NCC SEES graduate program for the financial research and software support.

I would also thank to METU NCC Mechanical Engineering Program for giving me a teaching assistantship position. It was truly a great opportunity and experience in order to improve myself. Also, I would like to thank all members of the program whom I worked with during this period.

Besides, I would like to thank all my friends and colleagues who always helped and supported me during this thesis study.

Lastly, I would thank to my family members my mother Sevgi Özel, my father İhsan Tuğrul Özel, my brother C. Noyan Özel and others who always supported me. This would not be possible without them.

Coşkun Kağan Özel

TABLE OF CONTENTS

LIST OF TABLES

LIST OF FIGURES

NOMENCLATURE

θ	Chiral angle	Degrees
v	Poisson's ratio	-
ϕ	Torsional angle	Radians
2α	Change in rotation angle	Radians
$\Delta\beta$	Twist angle	Radians
$\Delta\theta$	In-plane increment	Radians
$\Delta\tau$	Twisting angle increment	Radians
Δd	Change in diameter	nm
ΔL	Change in axial displacement	nm
Δr	Bond stretching variation	nm
A	Cross-sectional area	nm^2
a	Unit vector length	nm
C	Circumference of CNT	nm
C_h	Chiral vector	-
d	diameter	nm
E	Young's (Elastic) modulus	TPa,GPa
F	Force	nN
G	Shear modulus	TPa,GPa
I	Moment of Inertia	nm^4
J	Polar moment of inertia	nm^4
k	Force constant	nN/nm
$k\theta$	Bending resistance constant	nN/nm
$k\tau$	Torsional resistance constant	nN/nm
$k\tau$	Bond stretching resistance constant	nN/nm
L	Length	nm
m	Index of chiral vector	-
n	Index of chiral vector	-

R	Radius	nm
T	Torsion	Nn nm
t	Wall thickness	nm
U	Steric Potential Energy	J

Subscripts

θ	Bond angle
τ	Dihedral angle
bend	Bending
cnt	Carbon nanotube
CNTRP	Carbon nanotube reinforced composite
P	Polymer
r	Rule of mixture
SWNT	Single-walled carbon nanotube
str	Stretching
tws	Twisting

1. INTRODUCTION

1.1. Motivation

In the last century, increasing World population and rapid rise in industrialization have created huge damage in the ecosystem and the environment. Some of the main reasons for these damages are excessive material consumption and uncontrollable waste management. Therefore, this alarming situation attracts researchers to focus on more sustainable and eco-friendly alternative solutions. One of the potential alternative solutions can be use of nanocomposites instead of conventional materials due to their extraordinary physical properties [1]. Due to these superior properties of nanocomposites, researchers in multiple areas across the globe are studying nanocomposites exceedingly for the last two decades [2].

The discovery of carbon nanotubes (CNTs) go back to the year 1991 [3]. After the accidental discovery of CNTs by the Japanese scientist Sumio Iijima, CNTs become one of the most important and intriguing research topics among the researchers in various engineering and material science disciplines [4]. CNTs are very unique nanoscale tubular structures which possess exceptional physical properties such as mechanical, electrical, and thermal [2].

However, defects are common in carbon nanotubes, whose roles can be critical since they potentially distort the perfect hexagonal lattice structure of CNTs [5]. Defects can either occur during synthesis of CNTs or be formed after synthesis due

to environmental conditions. Several different types of defects can be seen in the CNT structures. However, the most common structural defects in CNTs are vacancies and Stone-Wales (SW) defects [6]. Therefore, effects of defects should be investigated in depth to understand their role in CNT's response to various loads and effects, and therefore to obtain more realistic results in modelling.

Their mechanical properties make them promising reinforcement fibres for nanocomposites. One of the most promising usage of CNTs are utilising CNT fibres as filler in a polymer matrix since combination of light weight of polymers with CNTs exceptional mechanical properties may result in an advanced material with desired properties [2]. These carbon nanotube-reinforced composites (CNTRPs) can be sustainable and eco-friendly alternatives for replacing conventional materials like aluminium and steel in various applications.

The applications of CNTRPs are new and mostly experimental nowadays. Although CNT based composites are promising; their abilities, properties are not completely understood. Extensive research studies should still be carried out to utilise CNTRPs in industrial applications. Studying on CNTs and other nanoscale materials can be rather difficult due to expensive synthesis techniques and the high technology required. However, thanks to the rapid development in computer science and engineering, computational methods offer researchers an alternative way to investigate nanoscale particles and structures via finite element modelling and simulations.

1.2. Geometry of CNTs

A pristine carbon nanotube can be defined as a seamless roll of a hexagonal carbon atom network with a high aspect ratio. CNTs are fibrous materials and due to the high aspect ratio they retain, they can be considered as one-dimensional structures. CNTs can also be considered as the rolled form of a graphene sheet. Moreover, CNTs can be separated from similar carbon-based structures due to their highly isotropic characteristics. In both graphene and CNTs, carbon atoms create a hexagonal structure and each carbon atom in the lattice covalently bonds to adjacent three atoms with sp^2 hybridization [7].

Geometric structure of carbon nanotube is different for each CNT. The geometric structure of CNTs depends on its chirality. Chirality of a CNT can be found by chiral vector ($\overrightarrow{C_h}$) or Chiral angle (θ) which are defined on the hexagonal structure of graphene sheet [8]. The chiral vector and chiral angle shown in Figure 1.1 on a hexagonal structure of graphene sheet.

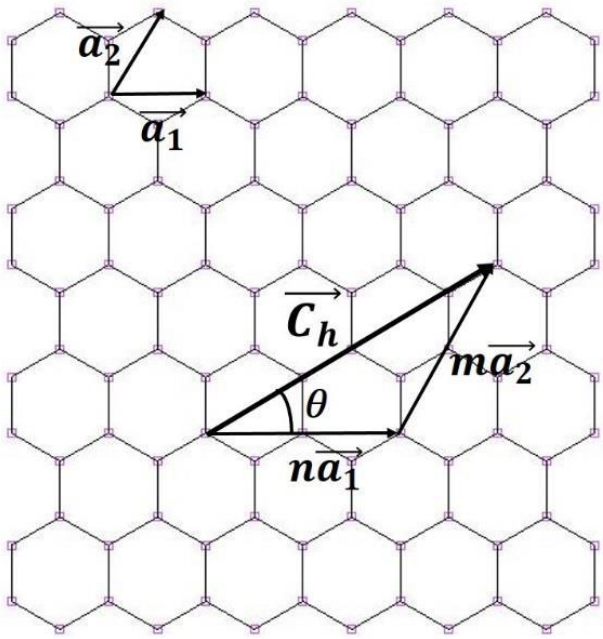

Figure 1.1 Chiral vector and chiral angle on a graphene sheet [9].

The chiral angle and chiral vector can be found through the Equations (1.1) and (1.2), respectively [8].

$$\theta = sin^{-1}\frac{\sqrt{3}}{2\sqrt{n^2 + nm + m^2}} \tag{1.1}$$

$$\overrightarrow{C_h} = n\overrightarrow{a_1} + m\overrightarrow{a_2} \tag{1.2}$$

Where n and m represents the chiral vector indices in integer which determines the chiral vector. Also, $\overrightarrow{a_1}$ and $\overrightarrow{a_2}$ are unit cell vectors with length of 'a'. The value of 'a' can found by Equation (1.3) [9].

$$a = \sqrt{3}\,L \tag{1.3}$$

Where 'L' represents the bond length between carbon atoms which is taken as 0.142 nm. Diameter of a CNT also depends on the chiral vector. Diameter 'd' and circumference 'C' can be evaluated by Equations (1.4) and (1.5), respectively. [9].

$$C = a\sqrt{n^2 + nm + m^2} \tag{1.4}$$

$$d = \frac{C}{\pi} \tag{1.5}$$

Based on their chirality, CNTs can be grouped in to three different categories as:

1) Armchair (n, n)

2) Zigzag $(n, 0)$

3) Chiral (n, m)

Table 1.1 summarises the CNT configurations for all three morphologies. Figure 1.2 shows those three different chirality configurations.

Table 1.1 Carbon nanotube morphologies with chiral angle and chiral vector

CNT Morphology	**Chiral Vector**	**Chiral Angle**
Armchair	(*n*,*n*)	30^o
Zigzag	(*n*,0)	0^o
Chiral	(*n*,*m*)	0^o < θ < 30^o

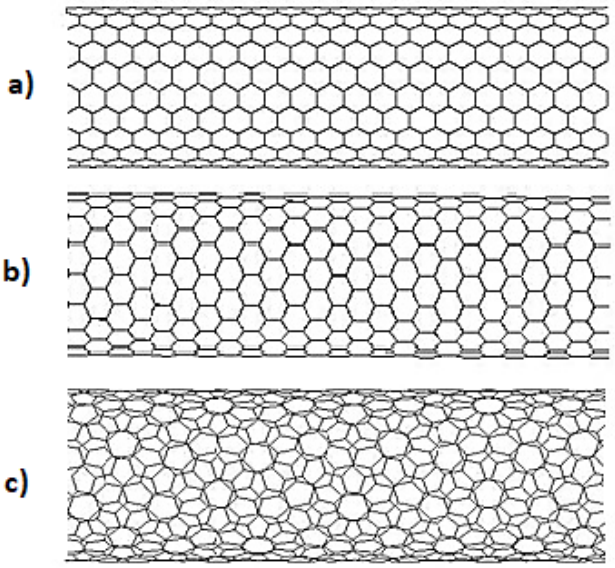

Figure 1.2 Models of different chirality CNTs where a) Armchair b) Zigzag c) Chiral

1.3. Types of CNTs

Carbon nanotubes can be grouped in line with the number of concentric tubes that they possess in the structure; namely as single-walled carbon nanotubes (SWNTs) or multi-walled carbon nanotubes (MWNTs) [10].

SWNTs are simply one rolled up graphene sheet into a cylinder where both ends are usually closed with a dome shaped half fullerene [11]. On the other hand, MWNTs should have more than one CNT structure concentrically and the ends of MWNTs can be open or closed. Moreover, there are covalent and/or van der Waals bond interactions between the concentric tubes [12]. Figure 1.3 shows the both multi-walled carbon nanotubes (MWNTs) and single-walled carbon nanotubes (SWNTs) [13].

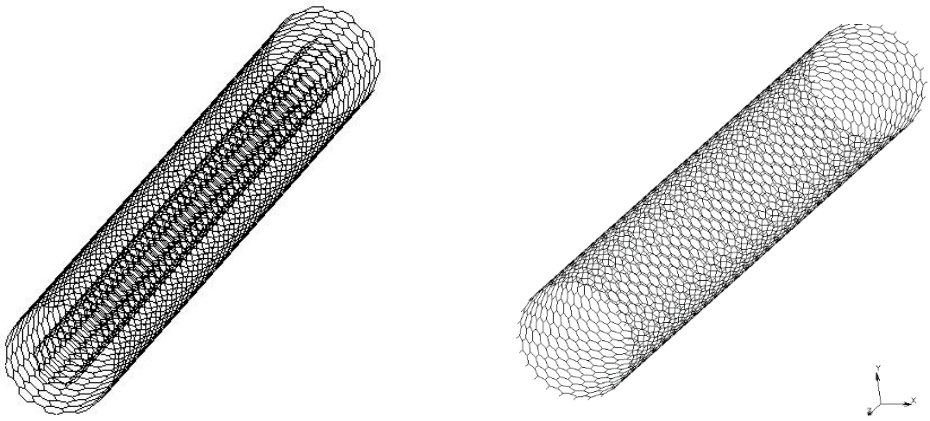

a) MWNT b) SWNT

Figure 1. 3 a) Computational model of multi-walled carbon nanotube and b) a single-walled carbon nanotube.

1.4. Mechanical Properties of CNTs

Soon after the discovery of CNTs, they have begun to attract many researchers all around the world due to their extraordinary material properties. C-C bonds are one of the strongest bonds in nature [7]. Moreover, highly isotropic structure of CNTs and sp^2 hybridization of carbon atoms make them very extraordinary in terms of mechanical properties like tensile strength, and elastic modulus. The tensile strength can be defined as maximum tensile stress that a material can handle before failure, which is very crucial for materials. Tensile strength of CNTs can reach up to around 200 GPa, where the value of tensile strength for some stainless steels is around 1.5 GPa [4]. Moreover, comparison of other similar strong materials in terms of tensile strength; i.e. graphite fibres, aramid (Kevlar),

etc. shows that CNTs possess much higher values. The comparison can be seen in Figure 1.4.

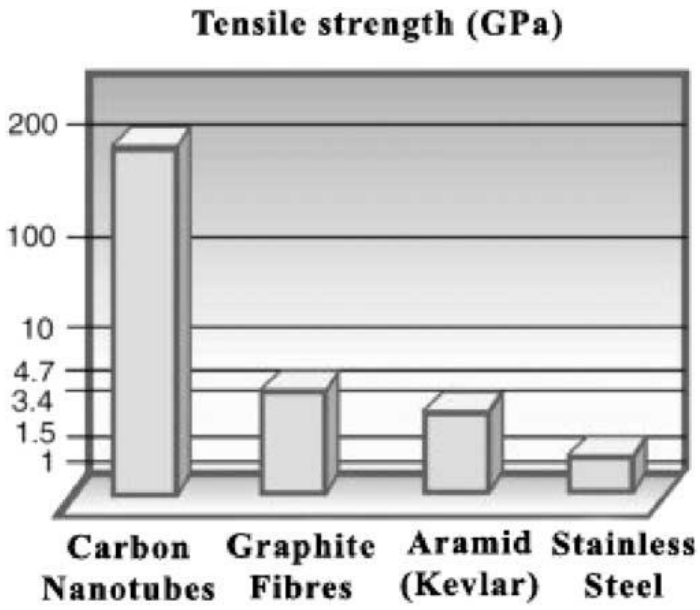

Figure 1.4 Comparison of selected materials for tensile strengths [4].

Elastic modulus, also known as Young's modulus, is another significant measure for mechanical material properties. Young's modulus can be defined as a measure of infinitesimal stiffness for an isotropic and elastic material. CNTs in general have high Young's moduli values when compared to similar materials. The reported values of Young's modulus for CNTs are alternating roughly between 1-5 TPa. On the other hand, the modulus value for carbon fibres is around 750 GPa [2]. These comparisons show that CNTs have great ability to resist deformation when compared to conventional materials.

Another mechanical property that should be considered is fracture strain value. The fracture strain value indicates the maximum strain before failure at the

fracture point. Fracture strain values are ranging between 10% - 30% for CNTs. In comparison with carbon fibres, the value lies between 0.1% - 2.0%. These figures demonstrate the ability for CNTs to withstand stress before fracture [2].

Therefore, beside the extraordinary mechanical properties like high tensile stress, Young's modulus, high fracture strain ratio; CNTs aspect ratio may reach around 10,000, and due to their unique structure, they have low density and weight compare to other known fibres [2]. Thus, all these properties and characteristics make CNTs great candidates as reinforcement fibres for composites such as CNTRPs.

1.5. CNTRPs as Advanced Materials

Nowadays, polymers are very common materials in our lives and all areas of the industry. Polymers are very popular due to their light weight and wide application areas. However, their mechanical and other physical properties are not enough to sustain desired conditions especially for structural applications. Although generally they have high ductility, their other critical mechanical properties are not as good as metals or ceramics. Thus, utilization of polymers for structural applications requires addition of reinforcement materials, particles, fibres, etc. [14].

Carbon nanotubes are great candidates as reinforcement fibres due to their unique tubular structural shape and nature of C-C bonds. CNTs also possess high aspect ratio with high strength to weight ratio. All these properties make CNTs

perfect filling materials for polymer composites. The carbon nanotube reinforced polymer (CNTRP) composites are very promising materials exhibiting unique compositions and advanced material properties. Tensile strength and stiffness values are generally high for CNTs. Therefore, addition of 1% of CNT to a polymer matrix by weight can increase tensile strength and stiffness around 25% and 40%, respectively [15]. Research studies show that tensile strength of CNTRPs can reach around 3.6 GPa. Moreover, elastic modulus also known as Young's modulus values can attain around 80 GPa [16].

CNTRPs are generally very light in weight, corrosion resistant, and strong materials. Also, recycling is possible and easy for CNTRPs since usually CNTs will not lose their unique structure and properties during common recycling processes. However, most of the polymers are not biodegradable and they are a huge threat for nature and environment. Thus, selection of polymer matrix is highly critical for CNTRP applications [2]. Epoxy resin can be one of the ideal selections due to its several advantageous in terms of sustainability. First of all, epoxy resin's adhesive properties are good. It can strongly bond with almost all surfaces. Only, some of nonpolar surfaces will not bond perfectly with epoxy resin. This adhesive bonding result in better fatigue resistance, and higher strength-to-weight ratio. Besides, epoxy resin with their light weight may help reduce cost in shipping and material consumption. Moreover, during subsequent processes in volatile solvents epoxy resin does not emit any volatiles. Recycling and studies on reuse of epoxy resin are premature nowadays. However, studies show that it is achievable with some

gasification processes. Also, CNTs can be extracted with recycling processes without losing their mechanical properties, after which they can be used for other applications [2].

Main application areas of CNTRPs for structural purposes are mostly related with aerospace and automotive industries. A theoretical case study with Euro Control's Base of Aircraft Data (BADA) shows that replacing aluminium flight profiles with CNTRP profiles may result in reduction of total weight around 14%. Also, it can provide almost 10% fuel saving with 13% increase in flight range [17]. Similarly, CNTRPs are very promising material for automotive industry. Use of CNTRPs in automobile bumpers is another possible application of CNTRPs. CNTRPs with their lightweight and proper mechanical properties will be good alternative material for the bumper systems. Compared to conventional fibre-glass bumpers 1 to 5% of CNT addition will be needed, where this value is almost 30% for fibre-glass bumpers [2]. Beside their mechanical properties and light weight, CNTRPs have also good conductivity. This will be useful for coating and painting since it will allow electrostatic spray applications. Furthermore, CNTRPs are already started to be used in sports industry. CNTRP based tennis rackets, and hockey sticks show superior performance [2]. Organic solar cell applications are another application area of CNTRPs. The solar cell applications of CNTRPs are very promising due to their superior optical and electrical capabilities.

1.6. Sustainability Aspects of CNTRPs

CNT synthesis is an energy intensive process when compared to the synthesis of conventional materials. For instance, when it is compared with aluminium the energy intensity can be larger in the range of 2 to 100 times more [18]. The CNT synthesis possesses many processes; i.e. purification, feedstock production, catalyst production, etc. All these processes should be considered for the energy consumption analysis. There are three main synthesis techniques for the CNTs which can be listed as chemical vapour deposition (CVD), arc discharge, and laser ablation techniques. All three techniques have their own advantages and disadvantages. Table 1.2 shows the basic comparison between these techniques.

Table 1.2 Comparison of CNT synthesis techniques [20][19][21]

Synthesis tech.	**CVD**	**Arc Discharge**	**Laser ablation**
Operation Temp.	<1200 ^{O}C	>3000 ^{O}C	>3000 ^{O}C
Operation Pressure	760-7600 Torr	50-7600 Torr	200-750 Torr
Advantages	Easy to scale up Low temperature	High quality CNTs Simple process	High quality CNTs High Purity
Disadvantages	Low quality CNTs More defects	Difficult to scale up Tangled CNTs	Difficult to scale up Expensive

As it is shown in Table 1.2 there are many differences between techniques. In addition to these differences, the cumulative energy requirements are also different from each other. Energy requirement of synthesis techniques compels investigation of sub processes for each technique in terms of thermal and

electrical energy. The sub processes can be listed as net feedstock, catalyst production, gas purification, arc/laser input, process heating, acid production, and purification processes. These sub-processes considered in terms of cumulative energy requirement of CNT production for CVD, laser ablation, and arc discharge can be seen in Table 1.3.

Table 1.3 Cumulative energy requirement for CNT synthesis [19]

Synthesis technique	**Thermal (MJ/kg)**	**Electricity (MJ/kg)**	**Total (MJ/kg)**
CVD	328	626	954
Laser ablation	300	2178	2478
Arc discharge	211	9624	9435

Although CNT synthesis is an energy intensive process, there are possible solutions to make the synthesis more sustainable and energy efficient. It is shown that solid waste hydrocarbons (post-consumer plastics) can be used for the low-cost alternative feedstock for CNT production [19]. Besides lowering the cost of feedstock, in industrial scale can be a sustainable and environmental solution for the solid waste hydrocarbons. Moreover, post-consumer waste hydrocarbons can be utilized as fuels due to their high heating values. When the solid hydrocarbons go under pyrolytic gasification process the result become mostly gaseous hydrocarbons and hydrogen mixture. This gas mixture can be considered as less polluting when compared to burning solid-state hydrocarbons. Furthermore, it is claimed that these gas mixtures can be used for combustion process to generate

power for CNT synthesis. [19] Thus, these by-product gases and possibility to generate power provide a chance to reduce energy demand of CNT synthesis. Figure 1.5 shows the flow chart of the CNT synthesis process from solid waste hydrocarbons.

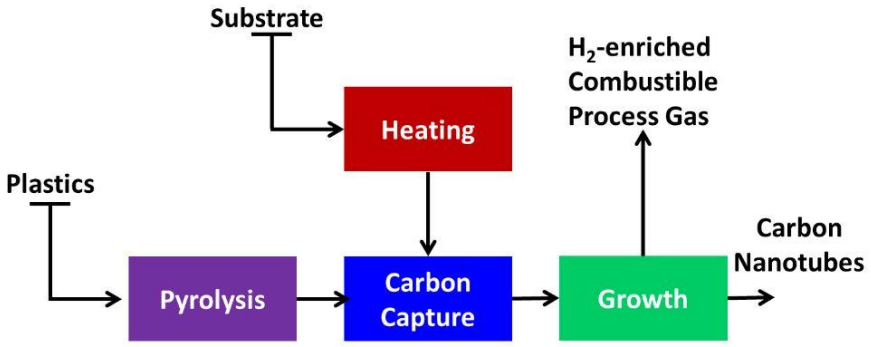

Figure 1.5 Flow chart of CNT synthesis from solid hydrocarbons [22]

Applications of CNTs are also important in terms of sustainability. One of the common applications of CNTs is carbon nanotube reinforced polymer (CNTRP) composites. CNTRPs can be considered as sustainable materials due to different aspects. CNTs have extraordinary physical properties and they retain their specific structure during subsequent processing. This makes recycling process possible for CNTRPs [20]. Recycling of polymers is very significant in improving cost effectiveness. Besides cost effectiveness, it is also important to reduce the stress on the environment in terms of pollution. Furthermore, CNTRPs are light in weight when compared to conventional materials which create many advantages such as less cost of shipping. In addition, study of Donnel et al. [17] shows that

replacement of airplane frame with CNTRPs results significant reduction in weight. It is shown that mass of air craft is reduced about 14% on average, which results in 9.8% fuel saving and 13.2% range increase on average. Usage of CNTRPs are not limited to structural purposes, emerging technologies shows that they can be also used to improve photovoltaic systems as organic solar cells.

Furthermore, use of CNTs allows for replacement of non-biodegradable polymers to biodegradable polymers. Utilization of biodegradable polymers is very significant to reduce the usage of petroleum-based polymers due to their degradability. On the other hand, in general biodegradable polymers have poor mechanical properties and low resistance to heat. Thus, CNT addition to biodegradable polymers can provide sufficient mechanical and thermal properties to composites [21].

1.7. Thesis Aims, Objectives and Overview

The first objective of this study to investigate the effects of the selected defects on different SWNTs using continuum-equivalent modelling for selected mechanical properties. A parametric study is conducted for different diameters and chirality configurations in order to understand the effects of CNTs on the selected mechanical properties. Furthermore, the second objective of the study is to model CNTRPs and to investigate the mechanical properties of the CNTRP models reinforced with defective CNTs.

The thesis study includes literature review in Chapter 2, where the studies related with defective SWNTs, synthesis techniques, CNTRP models, and the gaps in the literature are summarised. Chapter 3 discusses the methodology of finite element modelling of SWNTs and results for simulations. Next, Chapter 4 is the part where methodology and results for the CNTRP models are presented. Lastly, Chapter 5 is dedicated to discussion of conclusions and suggestion of possible future work.

2. LITERATURE REVIEW

2.1. Literature Review on SWNTs

CNTs have become very popular among researchers in related fields all over the world for last two decades. Especially, SWNTs are extensively investigated with both experimentally and numerically due to their better properties in terms of mechanical, electrical and thermal compared to MWNTs. Although there are experimental investigation techniques for SWNTs such as atomic force microscopy (AFM) and transmission electron microscopy (TEM), they mostly suffer from complexity and difficulties [22]. Moreover, experimental studies on this area are not cost- and time-effective when compared to computational methods.

Table 2.1 Literature review of SWNTs for selected parameters

Source and method	Diameter (nm)	Length (nm)	Young's modulus E (TPa)	Shear Modulus G (TPa)
Thermal Vibration [23]	1-1.5	23.4-36-8	~1.25	-
Ab initio [24]	0.8-2	-	0.8-1.22	-
Ab initio [25]	0.6-1.4	Infinite	0.5-0.82	-
Tight binding [26]	1.3	14	0.98	-
Equivalent Continuum model [27]	-	-	1.042	0.417
Equivalent Continuum model [28]	-	-	0.995-1.033	0.250-0.485
Equivalent Continuum model [29]	0.5-2.5	-	2.337	0.410

There are three main techniques to simulate CNTs numerically and they can be listed as; ab initio, molecular dynamics (MD) and equivalent continuum model (ECM) [30]. Ab initio is an effective and powerful approach compared to molecular dynamics for the small-scale systems. The main advantage of ab initio is the accuracy compared to molecular dynamics. However, computation with ab initio is expensive and only useful for small scale applications. On the other hand, molecular dynamics are better for large-scale simulations. With this method structure including 10^6 -10^8 atoms can be simulated around 10^{-8} seconds. Similarly, equivalent continuum approaches can be also use for domains include high number of atoms within reasonable time span [22], [30]. The continuum mechanics approach is also effective to simulate structures with non-linear behaviour like CNTs. Therefore, finite element method with equivalent continuum method becomes one of the best ways to simulate and analyse SWNT structures via computational modelling. Table 2.1 shows the selected studies in literature for different approaches both computationally and experimentally for SWNTs.

2.2. Literature review on defective SWNTs

Pristine carbon nanotubes are perfect tubular structures with hexagonal lattice of carbon atoms. The strength of C-C bonds and sp^2 hybridization of each carbon atom in the lattice gives the strength of carbon nanotubes. However, defects and disorders are common in carbon nanotubes [5]. There are several type defects that can be observed in CNTs. Most common structural defects in CNTs are

vacancies and Stone-Wales defects. Roles of structural defects can be critical since they potentially distort the perfect hexagonal lattice structure of CNTs. Defects can either occur during synthesis of CNTs or be formed after synthesis due to environmental conditions [5].

2.2.1. Stone-Wales Defects

After discovery of Stone-Wales (SW) defects in 1952, they have been studied extensively. SW defects are simply 90^{O} rotation of a C-C bond without changing the structural topography of CNT. SW defects formation energy is approximately 3.5 eV. Formation of SW defects do not affect sp^2 hybridization of C atoms. It only changes the adjacent hexagon structures. When, a SW defect occurs, it converts four adjacent hexagons into two pentagon and two heptagons [5][31]. A Stone-Wales defect on a CNT can be seen in Figure 2.1.

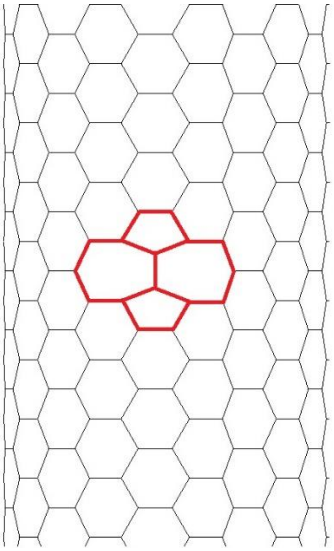

Figure 2.1 Stone-Wales defect on a SWNT

SW defect can occur during synthesizing processes due to condition of synthesis or after synthesis originating from environmental conditions (i.e. ion beam, electron radiation presence). Considering SWNT synthesis (at around 3000 K) the concentration of SW defects is around one SW defect per μm, on average [5][32].

2.2.2. Vacancy defects

Vacancies are the most typical and common defects in CNTs. Vacancy defects mostly occur after synthesis of CNTs. The reason is mostly environmental such as high energy ions, where neutron radiation may dislocate the C atoms. Vacancies are named by the number of missing atoms. Mono-vacancy (MV) and Di-vacancy (DV) defects are the most common types of vacancies. Figure 2.2 shows the mono-vacancy and di-vacancy defects on CNT structure respectively. Formation energy of mono-vacancy defects are reported as 7-7.8 eV and their concentrations are proclaimed according to synthesis temperatures of 1200 K (CVD) and 3000 K (Plasma) as 10^{-33} and 10^{-13} respectively [5][33]. In case of di-vacancies energy requirement for formation is lower than the mono-vacancies. It is reported that the formation energy for DVs are between 4.5 to 5.5 eV. Moreover, defect concentration of di-vacancies are given for 1200 K (CVD) and 3000 K (Plasma) as 10^{-22} and 10^{-9}, respectively [5][33].

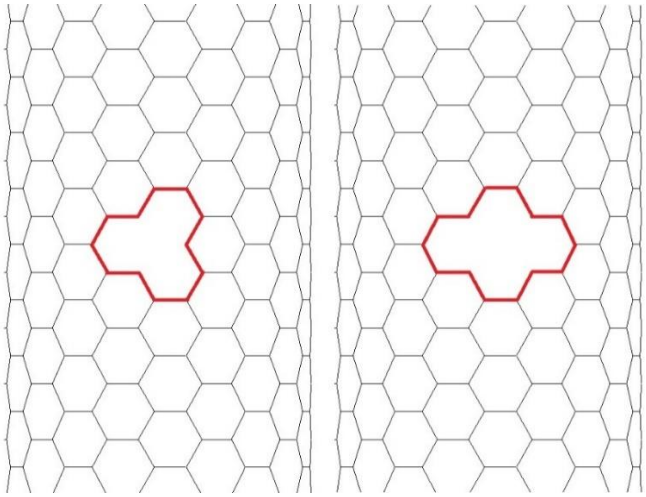

(a) **(b)**

Figure 2.2 a) Mono vacancy and b) di vacancy defects on a SWNT

2.2.3. Effect of defects on mechanical properties

Pristine CNTs pose extraordinary mechanical properties due to their unique structure. However, defects are common in CNT structures and to bring about a realistic point of view, they should be considered for the structural analysis. Defective CNT models have been studied in literature to see their effects on physical properties. Sharma et al. [34] studied on Stone-Wales and mono-vacancy defects on SWNTs by using molecular dynamics method. The study shows that presence of defects cause significant drop in mechanical properties. It is reported that presence of one mono-vacancy reduces tensile strength, tensile failure strain and Young's modulus by 22.61%, 34.17%, 3%, respectively for selected armchair configurations. Moreover, it is also reported that existence of one Stone-Wales defect reduces the same properties by 11.33%, 13.16% and 4%, respectively.

Another study [35] on vacancy defects shows that increase of vacancy defect up to 10% percent can affect Young's modulus up to 43% negatively. Similarly, presence of 10% vacancy defects increases Poisson's ratio about four times. In addition, in this study shear modulus is investigated and results shows that reduce in shear modulus in the same conditions can reach around 33%.

Furthermore, Lu and Bhattacharya [6] studied on randomly occurring SW defects on SWNTs. The study conducted on SWNTs of (6,6) and (10,0) configurations show randomly occurring SW defects between 1 to 4. Their results show that presence of one SW defect on SWNT (6,6) affects Young's modulus around 7% where this value is around 8% for SWNT (10,0). Moreover, in case of four SW defects presence the reduction in Young's modulus can reach around 15% and 16% for (6,6) and (10,0), respectively.

All these studies show that defects can be very detrimental on mechanical properties depending on types and concentration values. Thus, defective CNTs warrant further research in order to understand their effects and behaviour on mechanical properties.

2.3. Synthesis of SWNTs

There are huge amount research studies regarding large-scale synthesis of CNTs for industrial applications. However, heterogeneity of the sample is one of the main problems for large-scale production [36]. Other important problem is that it is difficult to control morphology and structure of CNTs. On the other hand, CNTs

can be synthesised by three main techniques for small scale applications. These three techniques can be listed as:

1. Arc Discharge
2. Laser Ablation
3. Chemical Vapor Deposition (CVD)

Besides these three main synthesis techniques, there are some alternative techniques that could be used for the synthesis such as molten salt technique, High Pressure CO Disproportionation Process (HiPCO), Plasma Enhanced Chemical Vapor Deposition (PECVD) [36].

2.3.1. Arc Discharge Technique

Arc discharge method is one of the basic methods to produce CNTs. This method is the main method to synthesize MWNTs. However, SWNT production is also possible with this method by adding metallic catalysts to system [37]. In this technique, carbon electrodes are used to generate arc. The two electrodes are placed with a distance between 1 to 2 mm as anode and cathode. In general, the diameter of the electrodes change between 5 to 20 mm [36]. The arc is generated due to different potentials between electrodes. The generated arc uses to vaporize carbon particles. The reaction occurs in an inert gas atmosphere (like He or Ar) at relatively low pressures when compared to other methods (50-700 mbar). Synthesis with this method requires high temperature inputs (Around 1700 ^{o}C) [36]. Similar to laser ablation this method also requires high energy input. Also,

usage of solid carbon source limits large-scale production like laser ablation method. Figure 2.5 shows schematic of the arc discharge technique.

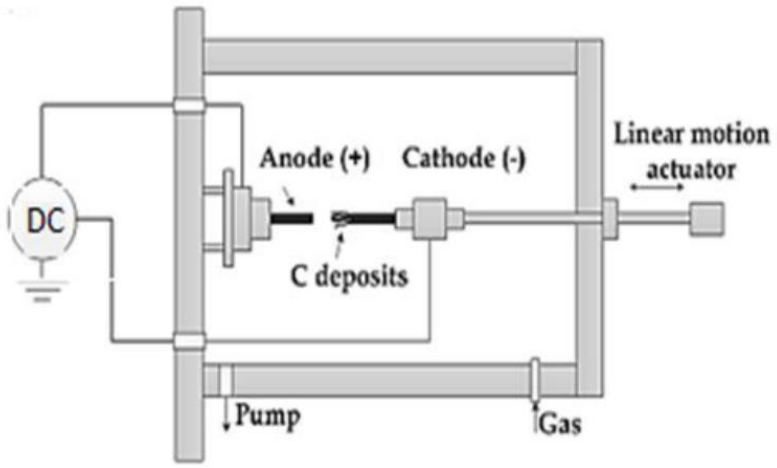

Figure 2.3 Schematic view of arc discharge [39].

2.3.2. Laser Ablation

Laser ablation method is another common synthesis technique for CNTs. In this method a laser beam is used to vaporize graphite as carbon source [36][38]. The reaction occurs in a quartz chamber at around temperature of 1200 ^{o}C and around 500 mbar pressure [36]. The vaporized carbon-based soot carried with flow of Ar or H_2 gas to water cooled copper collector. The soot may contain both SWNTs and MWNTs. However, laser ablation technique mostly uses to synthesize SWNT products. MWNT synthesis with this technique requires special conditions. Moreover, this method provides high quality tubes and better purity ratios compared to other two common methods. The purity ratio can reach up to 90% [36][37]. However, CNT synthesis with laser ablation method requires high energy

input. Also, requirement of solid carbon source (graphite) limits the production for large-scale processes [13]. In Figure 2.4 schematic of laser ablation technique can be seen.

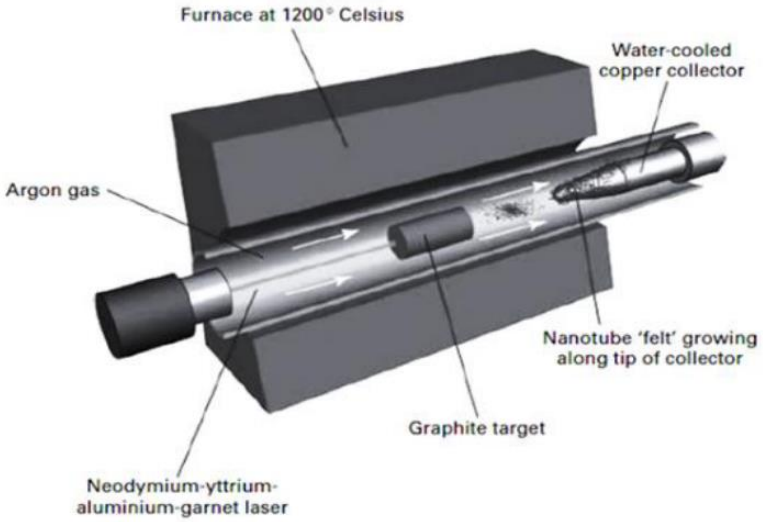

Figure 2. 4 Schematic view of laser ablation method [39].

2.3.3. Chemical Vapour Deposition

CVD synthesis compare to other two main synthesis techniques occurs in lower temperatures. With this synthesis technique both multi-walled carbon nanotubes (MWNTs) and single-walled carbon nanotubes synthesis can be done. Also, CVD technique allows to control morphology and structure of produced CNTs. In CVD technique gaseous form of hydrocarbons are mainly used as carbon source for nanotubes and the synthesis mainly occurs in atmospheric pressure [36][37].

CVD synthesis mainly occurs in a quartz furnace where this chamber involves a catalyst material. The furnace temperature changes between 550 ^{o}C to 1200 ^{o}C.

The flow of carbon source gaseous hydrocarbons with an inert gas (i.e. N_2, Ar) through to heated furnace will result in the synthesis of CNTs on the substrate surface [36]. The working conditions (i.e. temperature, pressure, concentration of carbon source gaseous, type and size of metallic catalyst etc.) of CVD affects the characteristic of CNTs. The length of nanotubes mainly depends of the reaction time. Moreover, number of walls can be controlled by alternating the temperature i.e. synthesis of SWNTs occurs in high temperature compare to MWNTs. Figure 2.3 shows the schematic of CVD process [36][13].

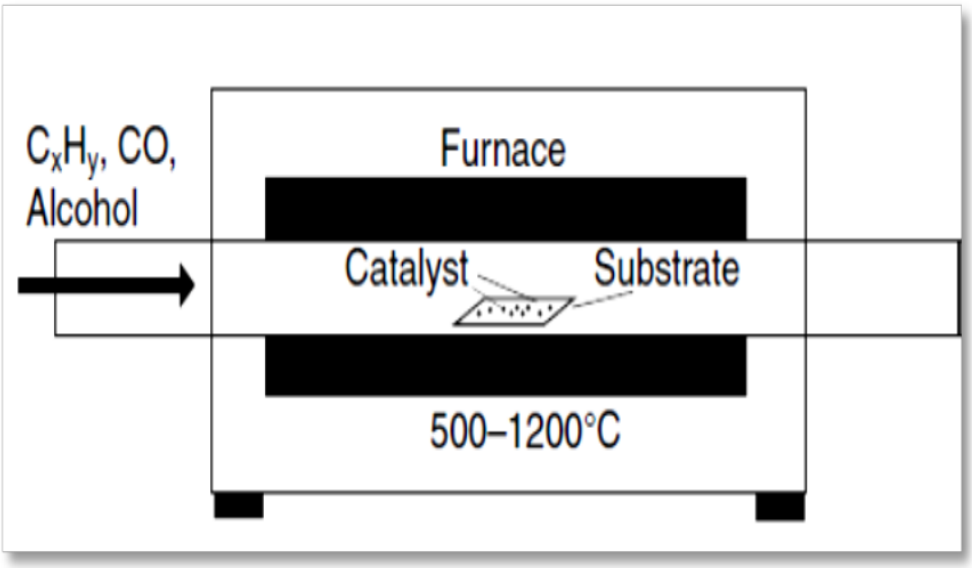

Figure 2. 5 Schematic of CVD system [39].

2.4. Literature Review on CNTRPs

In last decade, novel advanced engineering materials are increasingly used when compared to conventional engineering materials due to increase in scientific breakthroughs and rapid development in material science. Especially composite

materials have begun to play more critical roles in all areas of industry. However, their application areas are limited because of their restricted physical properties. Nano particle reinforced polymer composites (i.e. CNTRPs) are promising candidates with their improved physical properties to replace conventional materials. CNTRPs could be main structural material for automotive, aerospace, sport and renewable energy industries [17][39]. Studies on CNTRPs are common and extensive nowadays. However, usage of CNTRPs in industry applications, and large-scale production still requires major developments.

2.5. Synthesis of CNTRPs

Synthesis of CNT reinforced composites are still under development and it is a critical step to sustain desired properties. Dispersion of CNTs in polymer matrix is one of the problems to improve since CNTs can accumulate due to van der Waals interactions between them. There are three different ways to synthesize CNTRPs [16]. Solution mixing is one of them. In this method, CNTs are mixed with polymer matrix with mechanical mixing, high energy sonication or magnetic agitation. All these techniques help sustain the dispersion of CNT in the polymer matrix. Another common method is *in situ* polymerization. This method is very promising and an effective method to fabricate CNTRPs since it provides good dispersion of CNTs and effective interaction between polymer matrix and the nanotubes. In this method, polymerization of CNT-Monomer mixture is used to synthesize CNTRPs. Lastly, melt blend method can be used to synthesis CNTRPs. This method is mostly

common for the thermoplastic polymers. To apply this method, melted polymers are blended with CNTs to create CNTRPs.[16]

2.6. Finite Element Modelling Techniques for Simulating Defective CNTRPs

In literature, modelling of SWNTs for mechanical properties have been studied widely. However, studies on modelling defective CNTRPs for mechanical properties are scarce in literature. Therefore, limited amount of studies indicates the topic as a suitable area to work on. On the other hand, for the pristine CNTRPs, there are similar works done in the literature.

The study of Ayatollahi et al. [40] shows that working on representative volume element (RVE) to model the parts of CNTRPs can give realistic results under mechanic loads. They use the RVE models under tensile loads, bending and torsional loadings. The representative volume element used in study can be seen in Figure 2.6. The study is conducted for limited number of SWNT models in configuration of armchair and zigzag. Results indicate that effect of interphase is smaller on stiffness of CNTRP compared to the effect of length of SWNT and RVE.

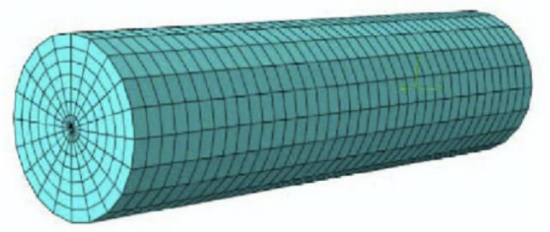

Figure 2. 6 Representative volume element (RVE) [43].

Study of Rafiee et al. [41] is another work on CNTRPs carried out to investigate crack propagation on CNTRPs. In this study, model of CNT created by equivalent continuum model for the configuration (10,10) SWNT. Moreover, model of interphase region created by solid elements instead RVE around CNT lattice for non-bonded interactions. Also, model of polymer matrix is created by solid elements around interphase region in rectangular shape. The model created for this study is shown in Figure 2.7.

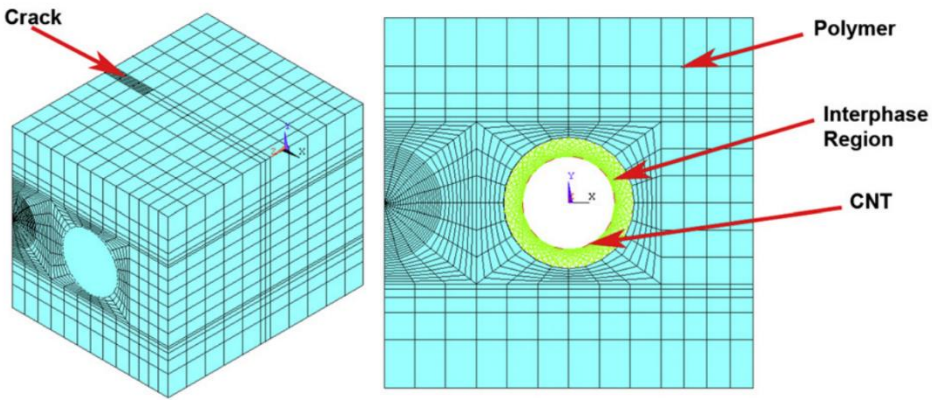

Figure 2. 7 Model of CNTRP with solid element interphase elements [44].

Furthermore, Rafiee et al. [42] presents modelling of CNTRPs in nanoscale for CNT and microscale modelling for polymer matrix with an interphase region model as van der Waals interactions. The models can be seen in Figure 2.8. The study aims to investigate impact and post-impact behaviour analysis of CNTRP structure and polymer. In simulations, CNTRP structure is subjected to mechanical loadings. The results show that in axial loading, deflection of neat polymer matrix is higher than the CNTRP around six times. With these results they claim that addition of small

quantities of CNT in polymer matrix increases the impact performance for non-bonded interaction interphases.

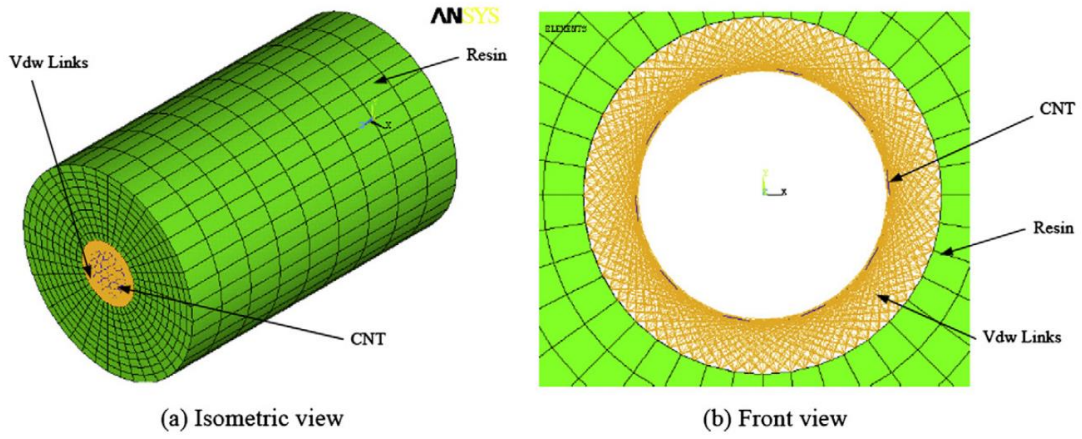

Figure 2.8 Isometric and front view of CNTRP with van der Waals interaction [45].

Beside the pristine CNTRP models, there are some studies conducted on defective carbon nano-tube reinforced composites. Gupta and Harsha [43] investigated defective CNTRPs. Their study includes vacancy defects (6, 9, and 10 atom vacancy) for SWNTs with configuration of (5,5) and (9,0). The interphase of model developed by using elastic cross links as representative of chemical covalent bonds between CNT and polymer matrix. The representative of CNTRP model can be seen in Figure 2.9. In addition, the study investigates the mechanical performance of the CNTRP under axial loading. Results show that increase of missing atoms in the lattice of SWNT reduces Young's modulus accordingly. It is also reported that armchair configuration gives better performance compare to zigzag configuration in terms of stiffness.

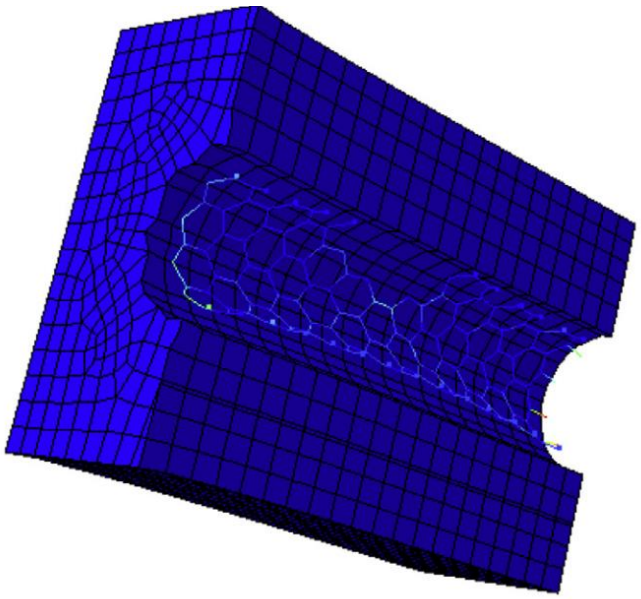

Figure 2. 9 Model of CNTRP for defective SWNT configuration [46].

Manboob and Islam [31] used molecular dynamics method to model their CNTRP structure. In this study they focused on defective SWNT reinforced Polyvinyl Alcohol (PVA) composites. They focused on mainly vacancy and Stone-Wales defects on their models. Their molecular dynamic model of CNTRP can be seen in Figure 2.10. Moreover, results show that presence of SW and vacancy defects in CNTRPs decrease Young's modulus by 2.0% and 2.6%, respectively.

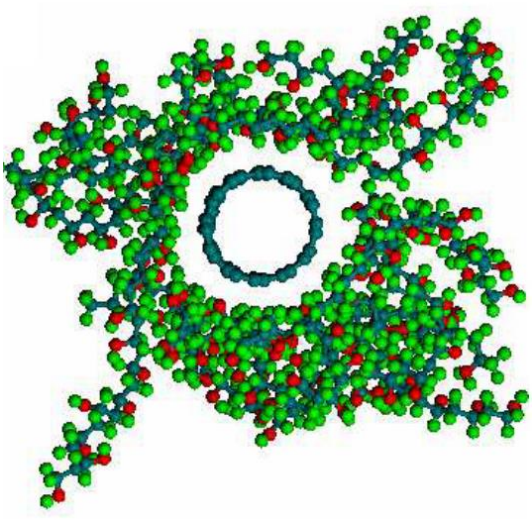

Figure 2.10 Molecular dynamic model of CNRTP [34].

2.7. Gaps in Literature

There are several studies in the literature that have been carried out on pristine SWNTs to investigate their mechanical properties. These studies mostly focus on investigation of mechanical properties of pristine SWNTs for limited chirality and diameters. It can be claimed that studies on defective SWNTs are mostly abstract and there are limited number of studies in the literature. These limited number of studies on defective SWNTs generally focused on single defect on SWNTs without a comprehensive parametric work in terms of chirality and diameters. Therefore, investigation of defective SWNTs possessing varying chiralities with a comprehensive parametric study for selected defects and their combinations creates a great opportunity for research. Moreover, similar to defective SWNTs, there is a paucity of research conducted on defective CNRTPs. Most of the studies

already carried out in this area mostly consider the perfect SWNTs in polymer matrices as filler fibres. There are very restricted and limited amount of studies has been published otherwise. Moreover, most of the work focused on single SWNT without a parametric study. Therefore, working on these gaps in literature offers a good research opportunity.

3. FINITE ELEMENT MODELLING OF DEFECTIVE SINGLE-WALLED CARBON NANOTUBES

3.1. Methodology

3.1.1. Equivalent-Continuum Modelling of Defective SWNTs

3.1.1.1. Molecular and Structural Mechanics

In graphene, SWNTs and MWNTs entire structure consists of carbon atoms and in between carbon atoms there are strong covalent bonds that keep them together. Under the effect of external loadings, these covalent bonds restrict their displacement and rotation with respect to each other. The total force between atoms mainly depends on electrostatic force between charged nuclei and force generated by electrons [22]. The total force can be generally expressed in terms of steric potential energy. Moreover, this total steric potential energy can be given as sum of energies related with bond interactions, valance, or non-bonded interactions. The total steric potential energy 'U_t' can be found the relation given in Equation 3.1 as a sum of corresponding energies [22], [44], [29].

$$U_t = U_r + U_\tau + U_\theta + U_w \tag{3.1}$$

These energies can be defined as follows: 'U_r' is bond stretching, 'U_τ' is dihedral torsion energy due to angle torsion, 'U_θ' is bending energy of the bond, and lastly, 'U_w' is the energy due to van der Waals bond interaction. These four parameters mainly constitute the total steric bond potential energy. However, when compared to bond stretching, dihedral torsion energy and bending energy, the

effect of van der Waals energy is small and generally omitted in the models. Rest of the energy parameters given above can be found via the following equations [22], [44], [29].

$$U_r = \frac{kr(\Delta r)^2}{2} \tag{3.2}$$

$$U_\theta = \frac{k\theta(\Delta \theta)^2}{2} \tag{3.3}$$

$$U_\tau = \frac{k\tau(\Delta \tau)^2}{2} \tag{3.4}$$

where the constants 'k_r', 'k_θ' and 'k_τ' indicate force, bond angle force, and torsional stiffness constants. And value of these constants are taken as 652 $\left[{}^{nN}/_{nm}\right]$, 0.876 $\left[{}^{nN \times nm}/_{rad^2}\right]$ and 0.278 $\left[{}^{nN \times nm}/_{rad^2}\right]$, respectively [28]. Moreover, 'Δr', '$\Delta \theta$', and '$\Delta \tau$' stand for variation on bond stretching, in-plane increment, and increment of angle of twist in the energy equations above, respectively. The schematics of molecular dynamics of bonds can be seen in Figure 3.1.

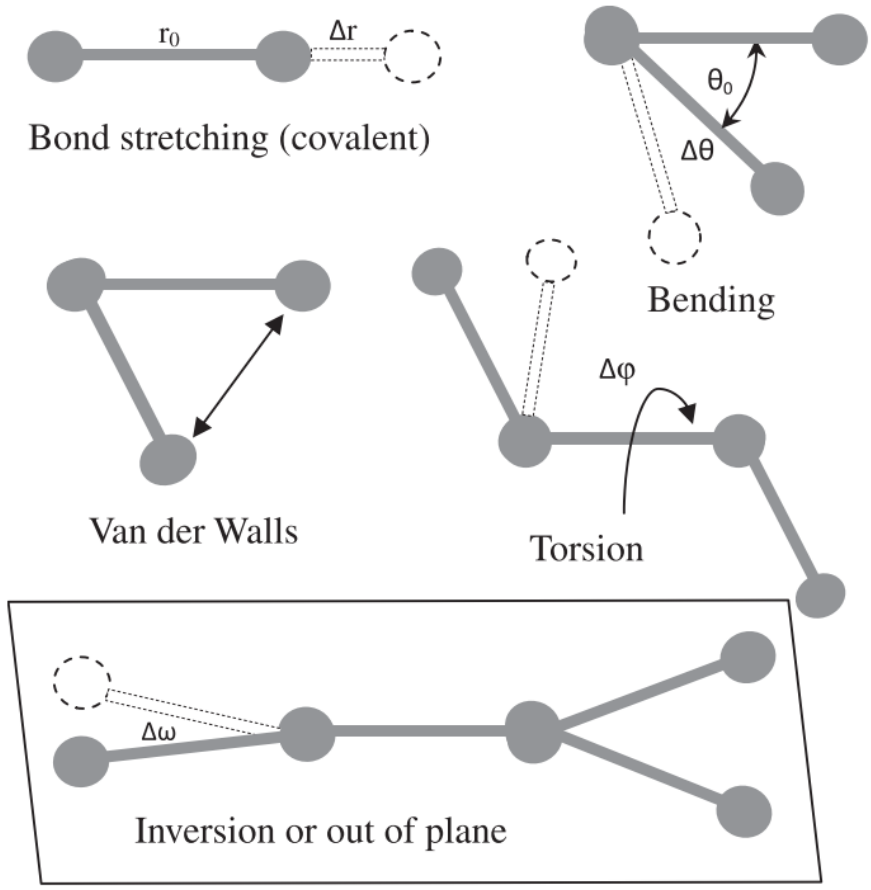

Figure 3.1 Schematic of atomic bond interactions in molecular dynamics [25].

Furthermore, consideration of carbon to carbon (C-C) covalent bonds as three-dimensional solid section beams with necessary abilities like bending, stretching and twisting allows to model C-C bonds with following equations [22], [44], [29].

$$U_{str} = \frac{EA(\Delta L)^2}{2L} \tag{3.5}$$

$$U_{bend} = \frac{EI(2\alpha)^2}{2L} \tag{3.6}$$

$$U_{tws} = \frac{GJ(\Delta\beta)^2}{2L} \tag{3.7}$$

Where '*E*' and '*G*' represent the Young's and shear moduli values, respectively. Moreover, '*I*' and '*J*' indicate moment of inertia and polar moment of inertia of the beam replacing the bond. Lastly, '*A*', and '*L*' stand for the geometric properties of the beam as cross-sectional area, and length of beam, respectively. Besides; $\Delta L, 2\alpha$, and $\Delta\beta$ represent deformation in axial direction, rotational angle change, and rotation of beam, respectively [22], [44], [29].

Moreover, the relation of Young's and shear modulus can be expressed as equations 3.8 and 3.9, respectively. Also, geometric properties '*A*', '*I*' and '*J*' with the assumption of circular isotropic beam with diameter '*d*' can be define as equations 3.10, 3.11 and 3.12, respectively [22], [44], [29].

$$E = {}^{4k_r L}/_{\pi d^2} \tag{3.8}$$

$$G = {}^{32\, k_\theta L}/_{\pi d^4} \tag{3.9}$$

$$A = {}^{\pi d^2}/_{4} \tag{3.10}$$

$$I = {}^{\pi d^4}/_{64} \tag{3.11}$$

$$J = {}^{\pi d^4}/_{32} \tag{3.12}$$

3.1.1.2. Finite Element Modelling of Defective SWNTs

Finite element modelling is widely used in literature in order to to investigate SWNTs and similar structures. Scarpa and Adhikari [44] used a continuum

equivalent model to simulate C-C covalent bonds by using three-dimensional beam elements. They developed an isotropic beam model with necessary geometric and material properties. Similar modelling methodology is also used in the study of Zuberi and Esat [45] , which are both validated. In this study, the modelling methodology by Zuberi and Esat [45] is used and adapted in order to develop defective SWNTs . The sectional properties of C-C bonds can be seen in Table 3.1.

Table 3.1 Geometric and material properties of the circular beam element model [48].

Young's Modulus (E)	Shear Modulus (G)	Poisson's ratio (v)	Bond Length (L)	Bond Diameter (d)
16.71 TPa	8.08 TPa	0.034	0.142 nm	0.0844 nm

The models are generated in MSC.Marc/Mentat 2018 environment, which is a nonlinear multi-physics finite element modelling and simulation software. Models are created by using solid section beams feature identified by the code (Type 98). Moreover, every node in the structure has translational and rotational degrees of freedom in all axes (x, y and z). In the model, effect of transverse shear, and responses for non-linear and linear effects are also investigated. Figure 3.2 shows the (15,0) model of SWNT with the interface of MSC.Marc/Mentat 2018.

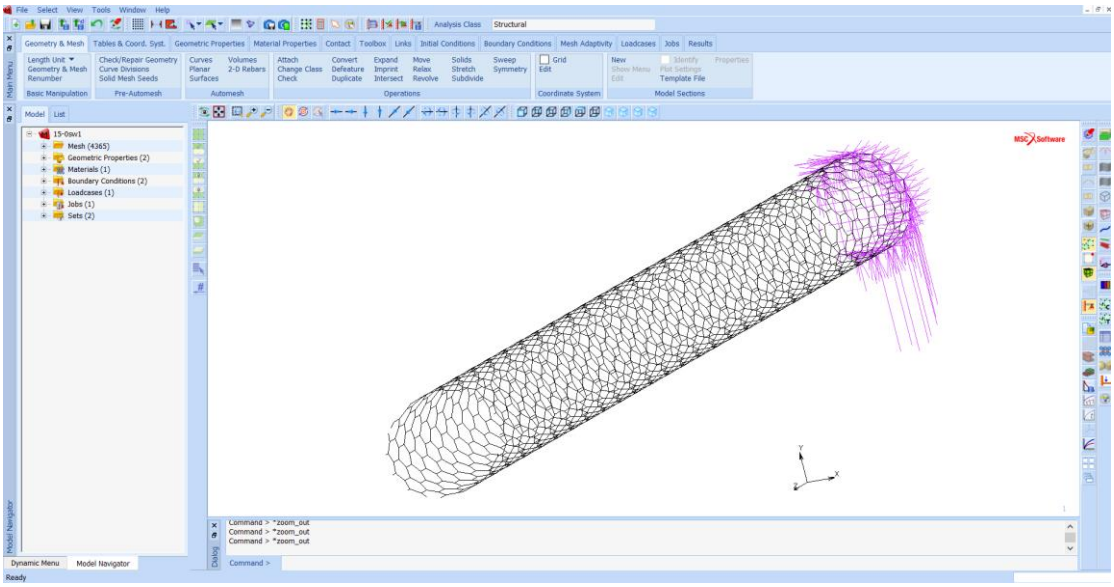

Figure 3.2 Isometric view of (15,0) SWNT and interface of MSC.Marc/Mentat 2018.

3.2. Results and Discussion

3.2.1. Evaluation of Young's Modulus of Defective SWNTs

Physical properties of CNTs depend on chirality and diameter as well as the mechanical properties. In this part; Armchair configurations for the tubes (6,6), (10,10), (12,12), (15,15), and (20,20), and Zigzag configurations for sizes (6,0), (11,0), (15,0), (20,0), and (25,0) are studied to demonstrate the effects of size of tube (in terms of diameter) on Young's modulus. Young's modulus is one of the most important mechanical properties for materials, indicating infinitesimal stiffness, especially for fibres. Young's modulus (also known as Elastic modulus) '*E*' is a measure of elasticity of a material in the elastic region. It indicates resistance to elastic deformation of a material under mechanical load. Young's modulus

evaluation is explained through the rule known as Hooke's law which depends on the linear relationship of between tensile stress 'σ' and tensile strain 'ε' values in elastic region. The Hook's law can be seen in Equation 3.13 [46].

$$E = \varepsilon\, \sigma \tag{3.13}$$

In case of SWNTs, Young's modulus calculation requires the values of the diameter of CNT, the initial length of tube, and the wall thickness of SWNT. The value of Young's modulus can be found through the following version of Hooke's law [22],

$$E = \frac{F\, L_O}{\pi\, d_{cnt}\, t\, \Delta L} \tag{3.14}$$

where, '*t*' is wall thickness of SWNT, '*F*' is applied force, 'L_O' shows initial length of the tube, and 'd_{cnt}' is the mean diameter of SWNT.

3.2.1.1. Wall Thickness Effect on Young's Modulus and Selection of Wall Thickness

Wall thickness is the one of the required parameters to determine mechanical properties of SWNTs such as Young's modulus. However, wall thickness of SWNTs is still under investigation. The studies in the literature for modelling SWNTs used varying values of wall thicknesses. Yakobson et al. [47] used the wall thickness value of 0.066 nm within molecular dynamics method. On the other hand, Odegard et al. [48] took this value as 0.69 nm for their equivalent continuum

mechanics model. Besides the extreme values, mostly assumed value for wall thickness is 0.34 nm since the value 0.34 represents the thickness of a single layer of graphene sheet [49]. This thickness value is taken and applied successfully for all molecular dynamics, tight binding, and equivalent continuum models in the literature. Therefore, in this study wall thickness for all SWNT models is taken as 0.34 nm. Moreover, Zuberi and Esat [49] investigate the effect of wall thickness on Young's modulus due to uncertainty in wall thickness. The parametric study on (10,10) armchair SWNT can be seen in Figure 3.3.

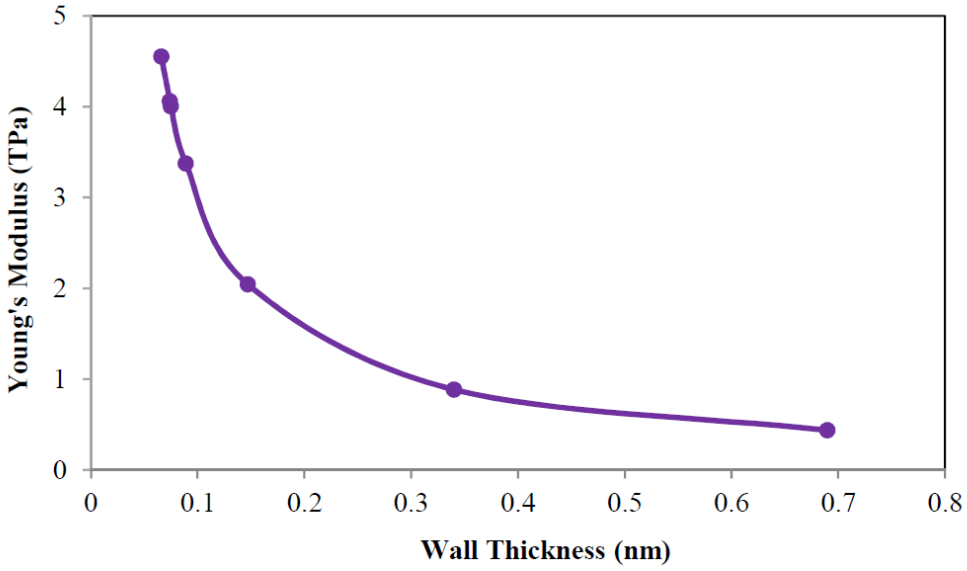

Figure 3.3 Change in Young's modulus with respect to wall thickness for (10,10) SWNT [49].

3.2.1.2. Effect of Defects on Young's Modulus of Defective SWNTs for Armchair Configuration

Armchair configuration SWNTs are modelled via equivalent continuum mechanics approach using finite element modelling technique. To obtain the reaction force, 0.1 nm displacement is given to one end of the tube while the other end fixed in all three dimensions. The boundary conditions can be seen in Figure 3.4.

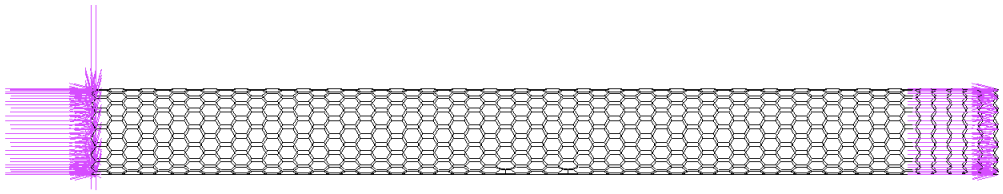

Figure 3.4 The boundary conditions for axial loading for (15,0) zigzag configuration.

Simulations are done for pristine version of SWNTs and for all selected three defect types, which are mono-vacancy (MV), di-vacancy (DV), and Stone-Wales (SW). Also, their combinations are applied to the models. Defects are located randomly to the mid portion of tubes.

Results show that, for the pristine tubes, the Young's modulus is almost constant for all diameter values simulated, which yields around 0.89 TPa. This shows the consistency of the armchair configuration with respect to change of diameter. Moreover, comparison of the calculated value of Young's modulus with the studies in literature shows good agreement. The studies of Meo and Rossi [50], Avila and Lacerda [51], Lu and Hu [22] reported that the average value of Young's modulus

is between 0.897-1.058 TPa. Furthermore, Figure 3.5 shows impacts of defects on Young's modulus for the defective and pristine models. It can be seen that randomly occurring mono-vacancy and di-vacancy defects individually affect the Young's modulus values in a similar fashion. Value of Young's modulus drops between 0.27% to 1.12% with respect to diameter for vacancies. However, when compared to vacancies, Stone-Wales defects affect the modulus value more significantly. Also, in this case, a considerable drop in Young's modulus for small diameters can be observed. The drop in the modulus alternates between 1.3% and 3.0%. In addition, randomly located combination of Stone-Wales and mono-vacancy defects are simulated. It can be claimed that presence of MV addition of a Stone-Wales drops the modulus value in the range of 0.22% to 0.81% with respect to single SW defect. Lastly, randomly located combination of all three defects are applied to the models. As expected, lowest value of Young's modulus values are obtained with this configuration. The decrease of the modulus value alternates between 2.15% to 6.38%. Thus, in this case the drop at the smallest diameter is significant. These results show that presence of defects affects the Young's modulus in small tubes more than the larger diameter ones. Moreover, presence of SW is more critical compared to the vacancies for armchair configurations. Chen et al. [52] investigated mono and di-vacancy defects on SWNTs for different diameters. Their results show that mono and di-vacancy follow very similar pattern. Moreover, drop of Young's modulus in terms of percentages are very close to the present work in presence of defects with change

in diameter. However, in the study values of Young's modulus are relatively higher when compared to the present work. Moreover, another study [6] on armchair configuration SWNT shows that presence of one randomly SW defect on (6,6) drops Young's modulus between 3% to 11%. These results are in good agreement with the obtained results in present study for armchair configuration.

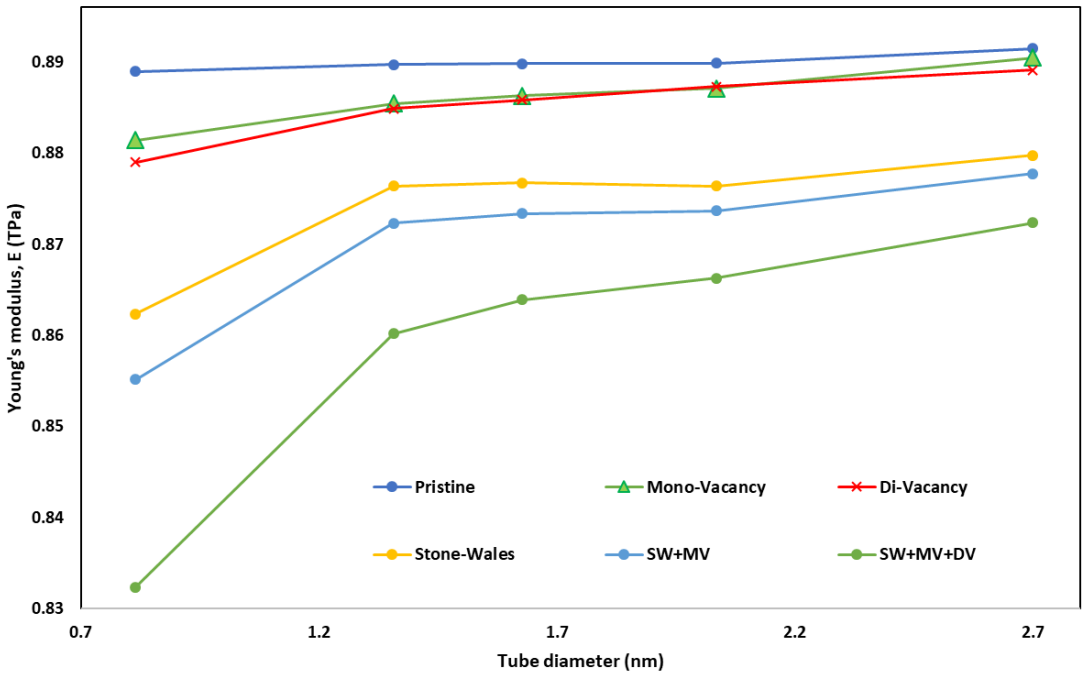

Figure 3.5 Variation of Young's modulus with respect to defect type and diameter for armchair configuration.

3.2.1.3. Effect of Defects on Young's Modulus of Defective SWNTs for Zigzag Configuration

Similar to armchair configuration, zigzag configurations are modelled with equivalent continuum model for the tubes (6,0), (11,0), (15,0), (20,0) and (25,0).

Same displacement value (0.1 nm) is applied to one end while the other is fixed to see their reaction under tension.

Pristine version of SWNTs for zigzag configuration are also modelled and simulated for a reference similar to armchair configuration. The results for the parametric study can be seen in Figure 3.6. In this case, on the contrary of armchair models, pristine SWNTs do not show the consistency with respect to diameter. There is a decreasing trend in Young' modulus with respect to decrease of diameter. However, presence of vacancy defects shows similar effects on the modulus in diameters larger than 0.8 nm. On the other hand, in small diameters their effect becomes much larger than that of SW defects. The decrease of vacancy defects in diameters larger than 0.8 is between 0.41% to 1.11%. However, their impacts on the tube (6,0) are 1.90% and 2.65% for mono-vacancy and di-vacancy, respectively. Besides, randomly occurring Stone-Wales defect on the tube creates drop on the modulus between 0.45% to 0.91% with respect to change in diameter. Furthermore, as expected, increase in defect concentration causes further drop in Young's modulus. For the presence of both MV and SW maximum change in the modulus is around 2.91% while the minimum value is 0.76%. Similarly, when all three type of defects occurring value of decrease in elastic modulus alternates between 1.2% to 5.2%. Study of Chen et al. [52] shows that effect of mono and di-vacancy defects have very similar patterns compared to the present study. On the other hand, drop in small diameters are more critical in the present study compared to the predictions of Chen et al. [52]. Lu and Bhattacharya [6] also

studied on zigzag (10,0) for SW defects. They claim that randomly occurring one SW defect can affect Young's modulus between 1.2% to 13%. The results of the studies in the literature are in good agreement with the predictions of the present study for zigzag configurations.

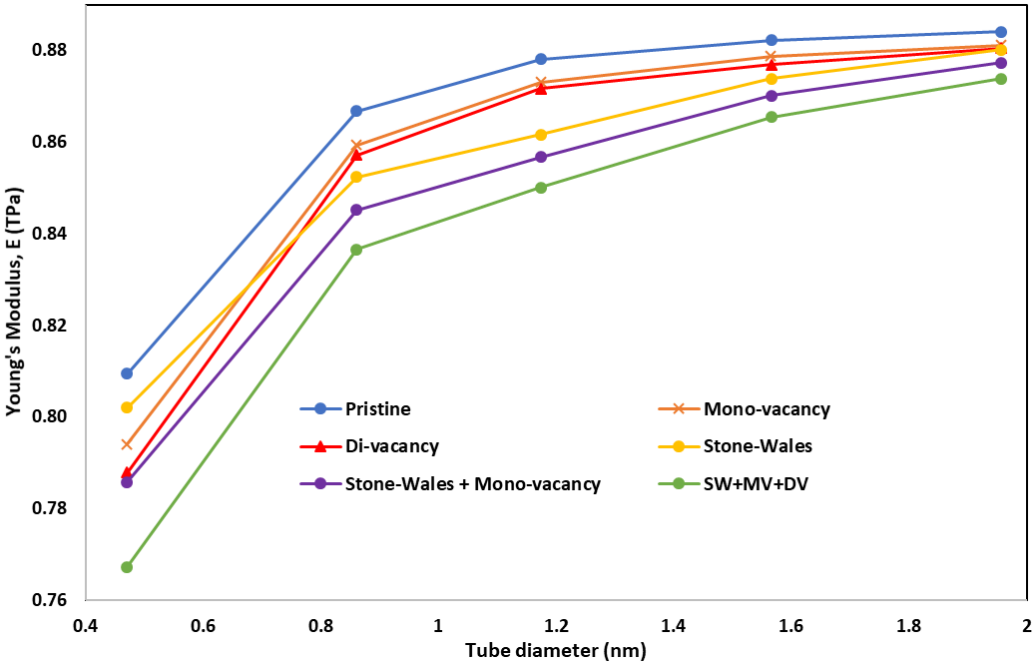

Figure 3.6 Variation of Young's modulus with respect to defect type and diameter for zigzag configuration.

3.2.2. Evaluation of Shear Modulus of Defective SWNTs

In this part of the thesis another important material property, shear modulus '*G*', of defective SWNTs is investigated. The investigation is done for the same defective and pristine SWNT models with Young's modulus analysis. The parametric analysis is carried out for the armchair and zigzag configurations for

diameter and defect type change. Shear modulus is a physical property and it can be determined by following equation.

$$G = TL/J\emptyset \tag{3.15}$$

'Ø' is angle of twist which is the rotational angle about the longitudinal axis that occurs due to torsional effect on SWNT. Moreover, '*L*' is the length of the tube, '*T*' is applied torsion load, and lastly '*J*' is polar moment of inertia for the cross-sectional area of SWNT. The polar moment of inertia of the tubes can be found by Equation 3.16.

$$J = \frac{\pi[(d+t)^4 - ((d-t)^4]}{32} \tag{3.16}$$

The representative of cross-sectional area of SWNT can be seen in Figure 3.7.

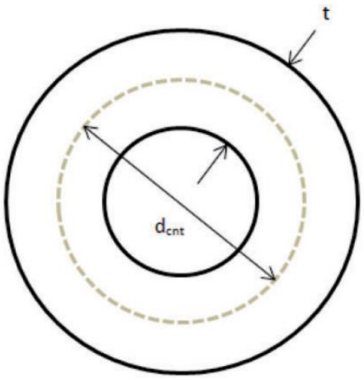

Figure 3.7 Representative view of cross-section of SWNT [52].

Furthermore, analysis of shear modulus is performed by applying torsion on tubes at one end while the other one is fixed. Effect of torsion to a SWNT can be seen in Figure 3.8.

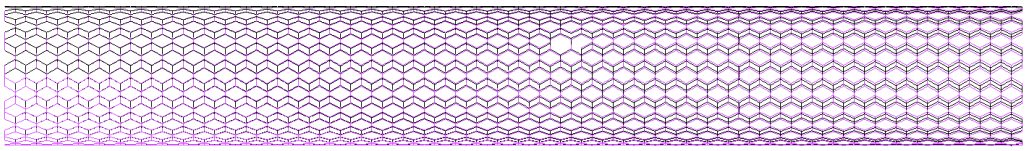

Figure 3.8 Deformed and undeformed view of (12,12) SWNT model under torsional load.

3.2.2.1. Effect of Defects on Shear Modulus of Defective SWNTs for Armchair Configuration

Armchair finite element models are used to determine shear modulus and investigate the effect of diameter and chirality. The models are observed under torsional load and shear modulus values are determined according to Equation 3.15. Results are given in Figure 3.9. The results show that pristine SNWTs gives the higher values for the shear modulus. Also, as it can be seen clearly in Figure 3.9 that presence of defects creates significant drop in the shear modulus. This drop is minimum for the mono-vacancy defects and its value is around 15% for diameters larger than 1.2 nm. Lowest value is obtained in higher concentration of defect case as expected. However, except MV, all defects have very similar effect on the shear modulus. Moreover, results show that for the pristine models shear modulus values merge around 0.4 TPa with increasing diameter. On the other

hand, for the defective SWNTs, this value is between 0.3-0.4 TPa. Chen et al. [52] show that mono and di-vacancy defects have similar effects on shear modulus. Also, in their work, drop in shear modulus with change in diameter appears to be close to the present study. However, results of Chen et al. [52] indicates that the value of shear modulus reach around 0.50 TPa, and 0.48TPa for pristine and defective SWNTs, respectively. Furthermore, effect of vacancy defects are investigated by Sakharova et al. [35] where they found that vacancy defects have similar effect on shear modulus.

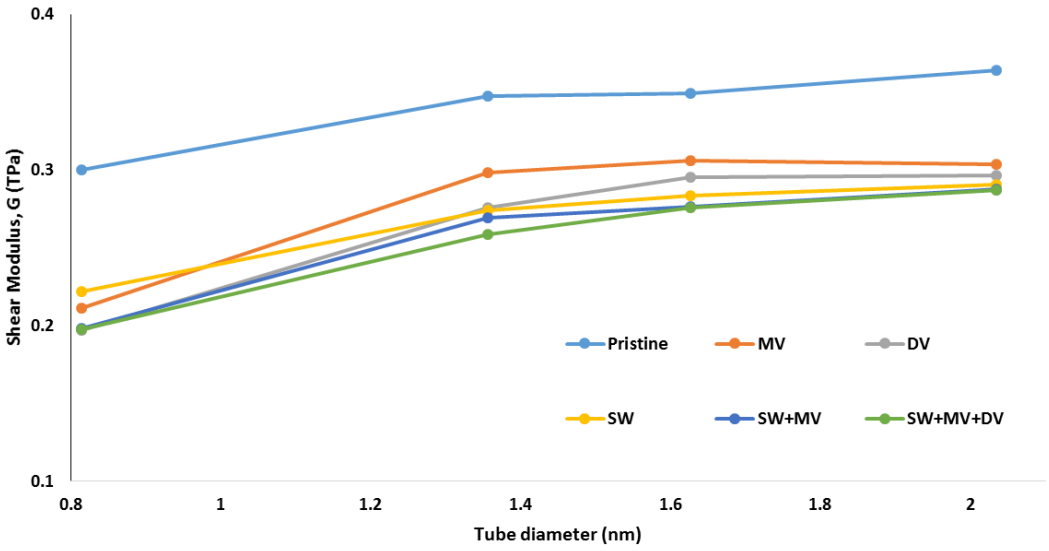

Figure 3.9 Variation of shear modulus with respect to defect type and diameter for armchair configuration.

3.2.2.2. Effect of Defects on Shear Modulus of Defective SWNTs for Zigzag Configuration

Zigzag model for all three type of defect and their selected combinations are used to determine shear modulus. Under torsional load models are investigated in a

similar manner to armchair configuration. Results for shear modulus with respect to diameter and defect types in zigzag configuration can be seen in Figure 3.10. Compared to armchair configuration, shear modulus values in this case appear to be under 0.4 TPa with increasing diameter. Moreover, the reduction of shear modulus is around 10% for the mono vacancy. All other defective structures follow similar pattern and are very close to each other. Studies by Chen et al. [52] and Sakharova et al. [35] on defective zigzag configurations for shear stress show that vacancy defects reduce the shear modulus in similar ratios when compared to present work. The values of shear modulus on the other hand are relatively different for each study. The shear modulus values are around 0.5 TPa, 0.45 TPa, 0.35 TPa for Sakharova et al. [35], Chen et al. [52], and present work, respectively.

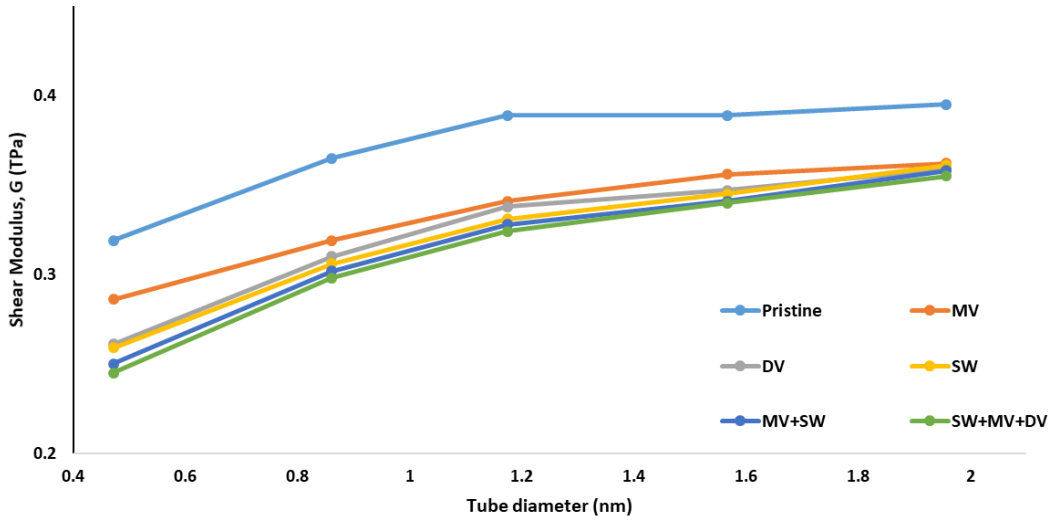

Figure 3.10 Variation of shear modulus with respect to defect type and diameter for zigzag configuration.

3.2.3. Evaluation of Poission's Ratio of Defective SWNTs

Similar to Young's modulus, Poisson's ratio mostly depends on the chirality and diameter of SWNTs. Same principle and models for both armchair and zigzag configurations are used with the analysis of Young's modulus in Poisson's ratio calculations. Poisson's ration 'ν' is an important mechanical property for the materials, representing the amount of change in deformation in varying axes of the specimen. It can be found by the following equation [46].

$$\nu = -\frac{\Delta d}{d} \times \frac{L}{\Delta L} \tag{3.16}$$

In the equation, '*d*' and '*L'* are the undeformed diameter and length of the SWNTs, respectively.

3.2.3.1. Effect of Defects on Poisson's Ratio of Defective SWNTs for Armchair Configuration

Poisson's ratios are found for the tubes (6,6), (10,10), (12,12), (15,15), and (20,20) for both defects and pristine tubes with armchair configurations. Results show that pristine SWNTs variation is small and consistent around the value of 0.250. Moreover, as expected, addition of defects cause significant changes to Poisson's ratio. Presence of randomly occurring Stone-Wales affects Poisson ratio consistently yielding increasing values between 14.73% to 23.39%. On the other hand, existence of vacancies in this case affect the Poisson's ratio much more than

the SW defect especially in smaller diameters. It is found that their effect might reach that up to 90.63% in small diameters. However, for the diameter 2.7 nm increase of Poisson's ratio is around 13.97%. Furthermore, increase of defect concentration gives much more differences in Poisson's ratio. All changes can be seen in Figure 3.11. The value of Poisson's ratio in small diameters and high defect concentration exhibit high and extraordinary values for the Poisson's ratio. This variation can be due to the space frame structure of CNTs. In small diameters,high concentration defect might result in huge empty spaces between atoms. Comparison with Sakharova et al. [35] shows that presence of vacancy defects increases Poisson's ratio by increasing concentration of defects. However, variation is small when compared to present study. Moreover, the value of the ratio is merging around 0.1 in their study.

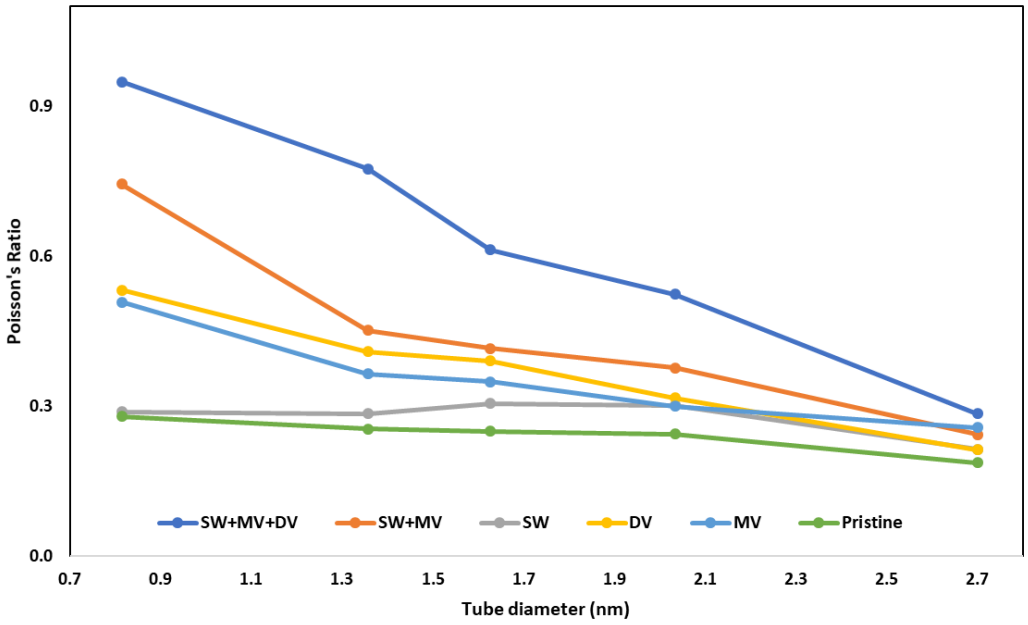

Figure 3.11 Variation of Poisson's ratio with respect to defect type and diameter for armchair configuration.

3.2.3.2. Effect of Defects on Poisson's Ratio of Defective SWNTs for Zigzag Configuration

Zigzag configuration is investigated for the chiral vectors (6,0), (11,0), (15,0), (20,0), and (25,0) using the same boundary conditions for the armchair configuration. In the case of zigzag configuration for pristine SWNTs Poisson's ratio values are around 0.250 for the tubes larger than 0.8 nm diameter. However, at the small dimeters the ratio reaches around 0.300. Moreover, for this chirality presence of defects affect Poisson's ratio differently than the armchair configuration. In this case, the difference between the defective tubes and pristine tubes are very high when compared to the armchair configurations. Stone-Wales defect configuration tubes show the closest pattern to pristine tubes in terms of

Poisson's ratio and their difference is between 37.03% to 39.74%. Furthermore, for the other defects and concentrations change in Poisson's ratio follows a very similar pattern. All the changes can be seen in Figure 3.12. Similar to armchair case, Sakharova et al. [35] study of zigzag configuration shows that effect of vacancy on Poisson's ratio is small and their value is around 0.1.

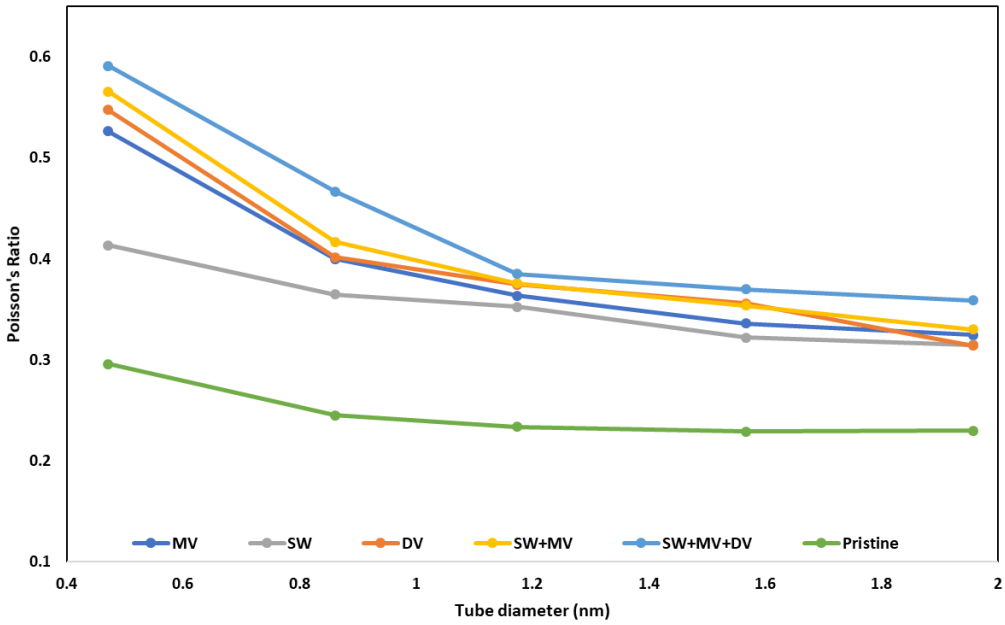

Figure 3.12 Variation of Poisson's ratio with respect to defect type and diameter for zigzag configuration.

4. FINITE ELEMENT MODELLING OF DEFECTIVE SINGLE-WALLED CARBON NANOTUBES REINFORCED POLYMER (CNTRP) COMPOSITES

This chapter mainly focuses on modelling of carbon nanotube reinforced composites (CNTRPs) and their simulation producing results for selected mechanical properties. In the previous chapter, defective SWNTs are studied for different chiralities (armchair and zigzag) and diameters. As a supplementary study in this chapter same SWNTs are used as reinforced fibres for polymer matrices to develop CNTRPs. Aim of this part is to investigate the performance of defective SNWT reinforced polymers.

4.1. Methodology

4.1.1. Modelling Representative Volume Element (RVE)

Representative volume elements (RVE) are a common finite element technique for the CNTRP models. In literature, this technique is used commonly to develop polymer matrix, interface and CNTs. RVEs can be in different shapes; most common ones are circular, rectangular, and polygonal cross-section shapes. However, in the current study circular models are used to develop CNTRPs. Moreover, to construct CNTRPs, defective SWNTs are used as filler material and epoxy resin as polymer matrix. Another important part of CNTRPs is the interphase region since it has a significant role in transferring stresses.

4.1.1.1. Polymer Matrix

Modelling of polymer matrices is a critical part of simulations since fracture of polymer matrices are higher than SWNTs in CNTRP structures. This fraction 'V_f' is around 4%. Therefore, modelling of polymer matrix via nano-scale atomic modelling requires high computational power due to high number of elements. On the other hand, continuum models can be used to develop polymer matrices as an effective solution. In this study, continuum modelling is used to construct polymer matrix as solid elements. The models are developed by using MSC.Marc/Mentat 2018 software.

4.1.2. Interphase modelling

Modelling of interphase region is important since it is a critical region to transfer stresses and loads between SWNT and polymer matrix. In the literature there are two main approaches to model the interphase region. These approaches can be listed as;

1. Discrete modelling approach, and

2. Continuum modelling approach

4.1.2.1. Discrete Modelling Approach

In this approach model interphase is considered as non-bonded van der Waals interactions between SWNT and polymer matrix. Therefore, discrete elements are

used to develop these interphase regions. Although some of the models are developed by beam elements in the literature, discrete elements are mainly utilised by employing spring/truss elements between SWNT and polymer matrix.

This model is studied in literature to model CNTRP models. Wernik and Mequid [53] used non-bonded interactions to determine the Young's modulus. The approach is also investigated by Zuberi and Esat [54]. Both studies show that it is a suitable approach to model CNTRPs.

4.1.2.2. Continuum Modelling Approach

Another approach is the continuum model. In this approach, perfect bonding condition is assumed for polymer matrix and SWNT. With this approach all SWNT, polymer matrix and interphase regions can be modelled with RVE models as linear, isotropic, and homogeneous materials.

This approach is used in literature to model CNTRP structures. Karimzadeh et al. [46] studied on CNTRPs with perfect bonding model. They worked on cubical RVEs beside cylindrical RVEs for elastic properties. Moreover, Rafiee et al. [41] used perfect bonding method to model CNTRPs. Lastly, Zuberi and Esat [54] shows that it is a valid method to model CNTRPs for obtaining mechanical properties.

In this study continuum modelling approach is used to model CNTRPs by using MSC.Marc/Mentat 2018 software. In Figure 4.1, continuum approach model of CNTRP generated in this study can be seen.

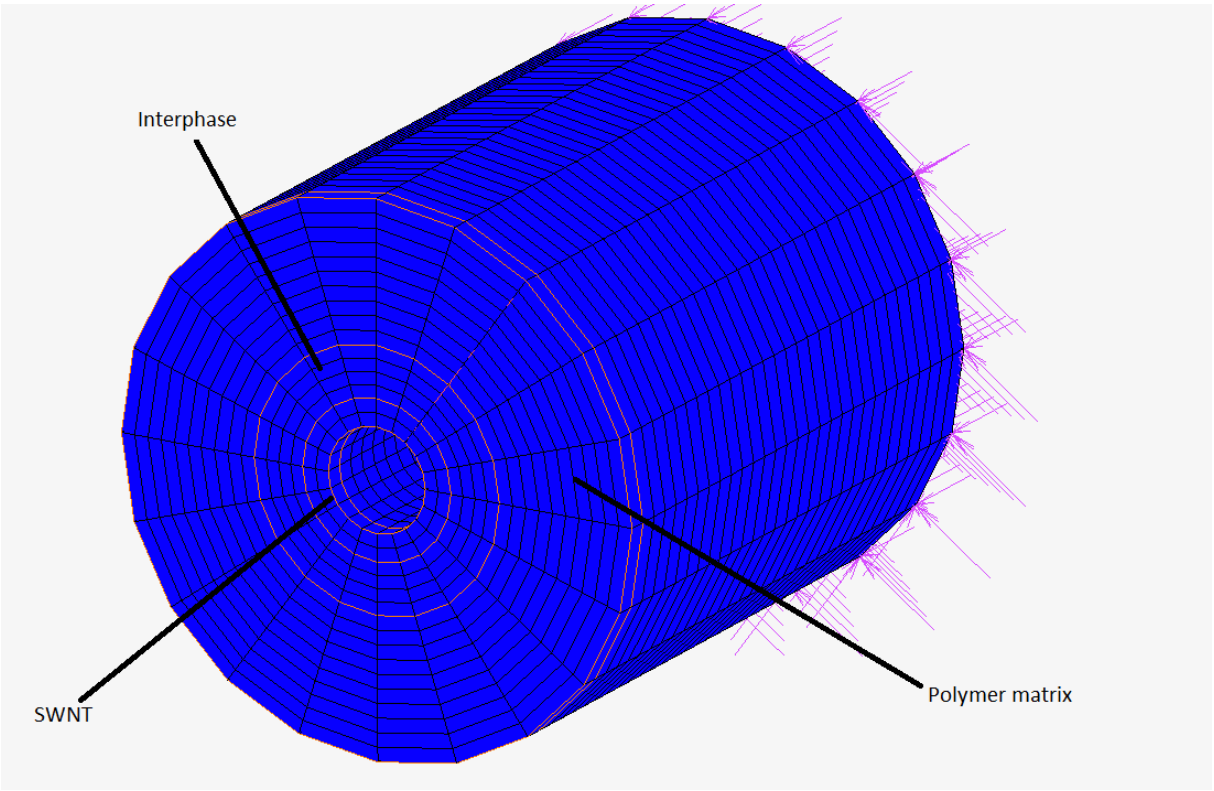

Figure 4.1 RVE model for perfect bonding approach

4.1.3. Model Validation

Models created computationally should be validated for realistic predictions. Continuum modelling approach RVE is validated before use in simulations against to literature. Moreover, analytical rule of mixtures method is used to validate models.

First of all, armchair (10,10) configuration is modelled and tested under axial loadings. This simulation is used to determine elastic characteristics of RVE model and the Young's modulus of RVE. To determine Young's modulus, RVE models are fixed in one end and displacement is applied at the other end. The applied

boundary conditions can be seen in Figure 4.2. Therefore, using the linear relationship between stress-strain also known as Hooke's law, Young's modulus can be found. The relation for Young's modulus can be found in Equation 4.1 [40];

$$E_{RVE} = F_{RVE} \times L_{RVE} / A_{RVE} \times \Delta L_{RVE} \quad (4.1)$$

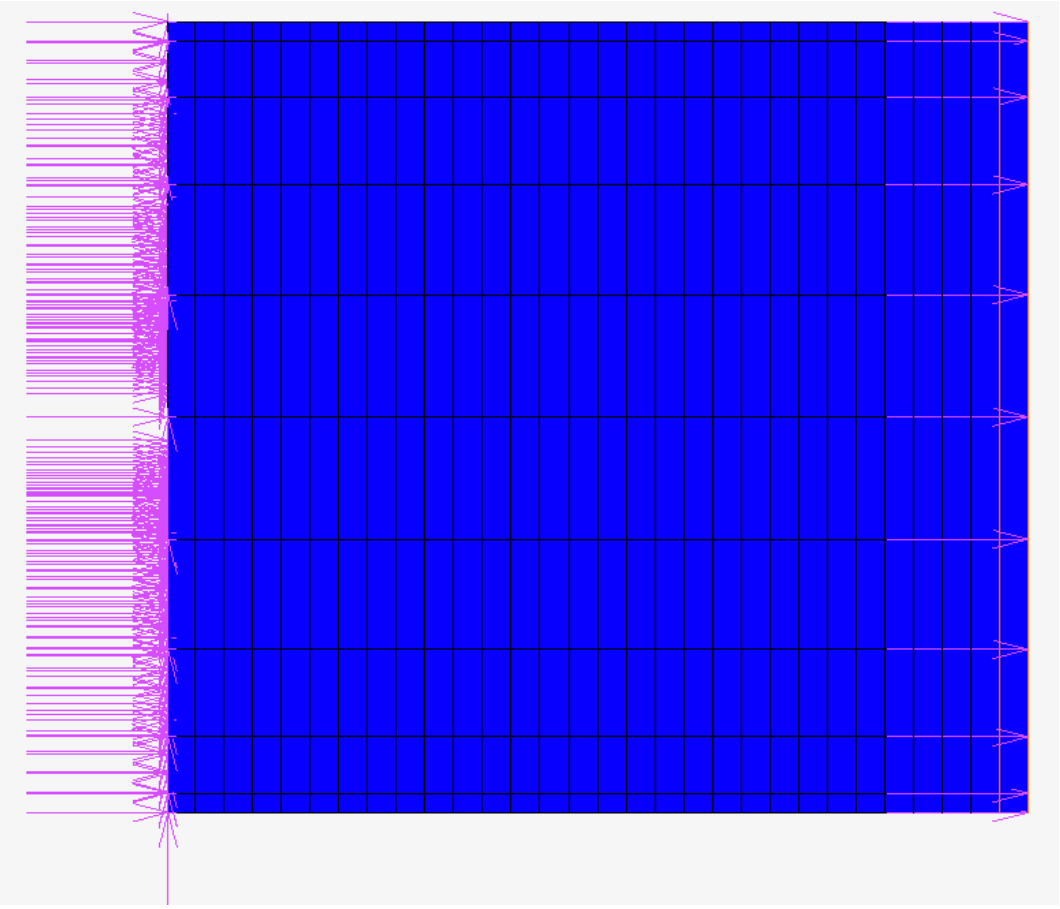

Figure 4. 2 Boundary conditions applied to RVE model

where 'F_{RVE}', 'L_{RVE}', and 'A_{RVE}' are axial reaction force, initial axial length of the RVE, and cross-sectional area of the RVE, respectively. Thus, result of simulations gives that Young's modulus of RVE as 54.5 GPa on average. Moreover, in the literature Karimzadeh et al. [46] and Rafiee et al. [41] studied on perfect bonding approach

for CNTRPs with 3% and 5% volume fraction values, respectively. Young's modulus values found in these studies are for Karimzadeh et al. [46] 53.5 GPa, and for Rafiee et al. [41] 56.5 GPa.

The second part of validation is carried out by the rule known as rule of mixtures. This method is mainly used for composite materials in order to determine their Young's modulus analytically. The relation of rule of mixtures for Young's modulus can be found in following equation [46], [55], [53];

$$E_r = E \times V_f + E_P(1 - V_f) \tag{4.2}$$

where 'E_r', 'E', 'E_P' represents Young's moduli of CNTRP, fibrous material (SWNT), and polymer matrix, respectively. Therefore, using rule of mixtures Young's modulus is calculated as 53.6 GPa on average. Thus, calculated values of Young's modulus via Hooke's law and rule of mixtures give close results. Moreover, values found in the literature coincide with a small variation. Therefore, these results appear to validate the created continuum model via perfect bonding model.

4.2. Results and Discussion

4.2.1. Evaluation of Young's Modulus of Defective SWNTs for Armchair Configuration

Evaluation of Young's modulus for CNTRPs is conducted by perfect bonding model RVE models. In armchair configuration, four different SWNT diameters are

considered to investigate Young's modulus. The simulations are conducted for randomly occurring SW, MV, DV, and their combinations. Moreover, pristine version of SWNTs are used as a reference point for all diameters. The results for armchair configuration can be seen in Figure 4.3. The results indicate that pristine CNTRPs have higher Young's modulus values compared to defective ones and its value is around 54 GPa with respect to change in diameter. On the other hand, presence of vacancy defects causes a slight drop in Young's modulus. Range of this drop is between 0.3% to 2.3%. However, addition one randomly SW defect to pristine tubes has larger effect on Young's modulus. In this case the modulus decreases between 1.1% to 5.5%. Besides, as the graph indicates clearly, drop in Young's modulus values increases with increasing defect concentration. It can be seen the value drops to around 46 GPa in small diameters.

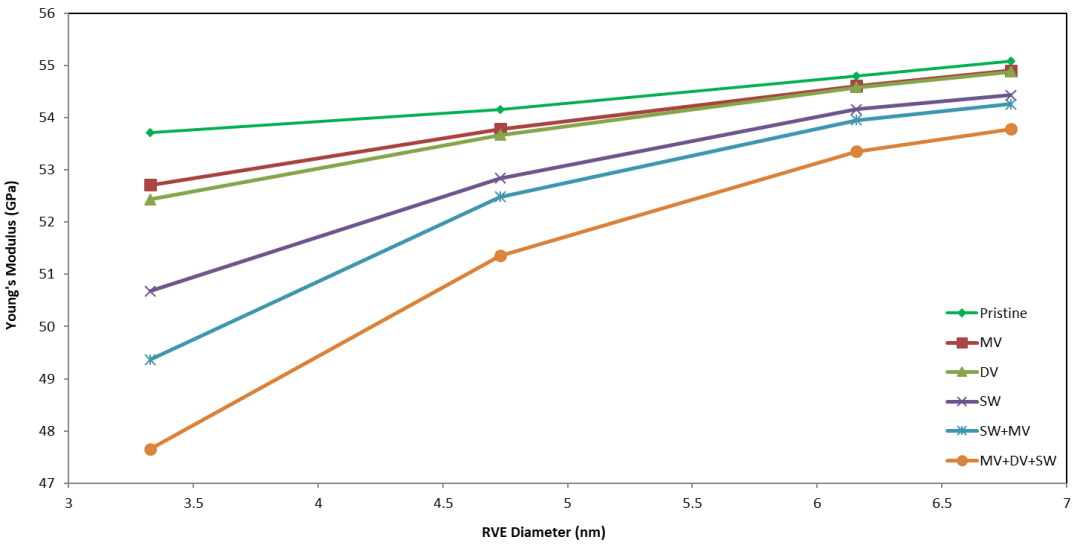

Figure 4.3 Variation of Young's modulus with the diameter for selected defect combinations for armchair configuration

4.2.2. Evaluation of Young's Modulus of Defective SWNTs for Zigzag Configuration

Investigation of effects of zigzag chirality on Young's modulus is carried out in this part. Same defect types and concentration are used with the armchair configuration for the selected four different diameters. Moreover, Young's modulus values of pristine SWNTs are found and reported as a reference data set. The results for Young's modulus are given in Figure 4.4 with respect to diameter change. The main difference with the armchair configuration truns out to be that there are decreasing trends in small diameters even in pristine SWNTs. In general, vacancy defects have similar effect on Young's modulus in zigzag configuration. Besides, similar to armchair configuration, the modulus values decrease with increasing concentration. For the maximum concentration ratio this drop is between 1.5% to 8.2%.

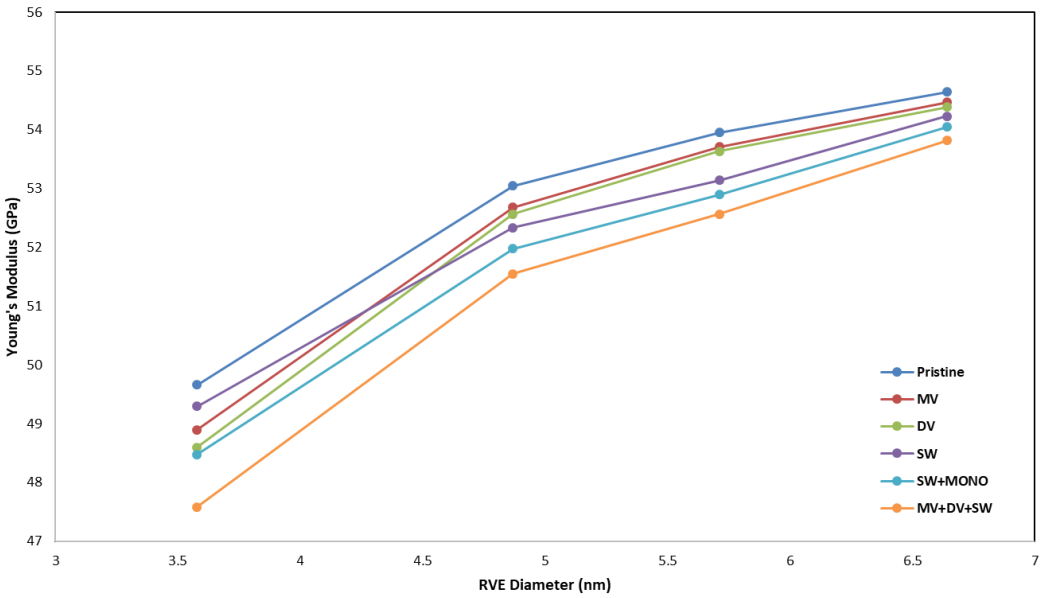

Figure 4. 4 Variation of Young's modulus with the diameter for selected defect combinations for zigzag configuration

4.2.3. Evaluation of Poisson's ratio of defective CNTRPs

Poisson's ratio is investigated in this part for defective CNTRP structures. Zigzag and armchair models are used for four different selected diameters. Different type of defects and concentrations are studied to understand the effects on Poisson's ratio. Poisson's ratios are calculated for CNTRPs via Equation 4.3 [46];

$$\nu_{CNTRP} = -\left(\frac{\Delta d_{CNTRP}}{d_{CNTRP}}\right) \times \left(\frac{L_{CNTRP}}{\Delta L_{CNTRP}}\right) \tag{4.3}$$

where 'd_{CNTRP}', and 'L_{CNTRP}' represent diameter of CNTRP and initial length of CNTRP, respectively.

4.2.3.1. Evaluation of Poisson's Ratio of Defective CNTRPs for Armchair Configuration

Investigation of Poisson's ration is conducted under similar conditions with the Young's modulus study. Therefore, one end of RVE is fixed against displacement in all three axes and axial displacement is applied to the other end. For the armchair configuration, same models are used to investigate the Poisson's ratio. Four different diameter SWNTs are studied and results are given in Figure 4.5. As the results indicate, Poission's ratio of pristine tubes decrease with increasing diameter and values fluctuate between 0.32% to 0.25%. Moreover, addition of defects causes the increase in Poisson's ratio. The increases are small for the diameters larger than 4.5 nm and the value is around 2%. However, in small diameter this increase reaches up to 19%.

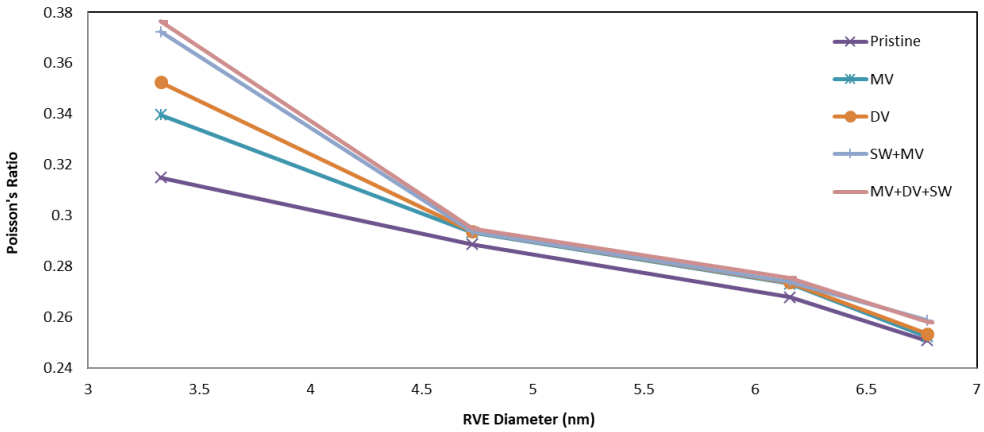

Figure 4.5 Variation of Poisson's ratio with the diameter for selected defect combinations for armchair configuration

4.2.3.2. Evaluation of Poisson's Ratio of Defective CNTRPs for Zigzag Configuration

The investigation of Poisson's ratio is also carried out for the zigzag configuration under the same conditions. Four different diameters are considered for the analysis. The results for the zigzag configuration for Poisson's ratio can be seen in Figure 4.6. In this case, results for all diameters follows a linear pattern and the values are very close to each other. Maximum variation is smaller than 1%. This result shows that zigzag configuration is very stable in case of occurring random defects on them for Poisson's ratio.

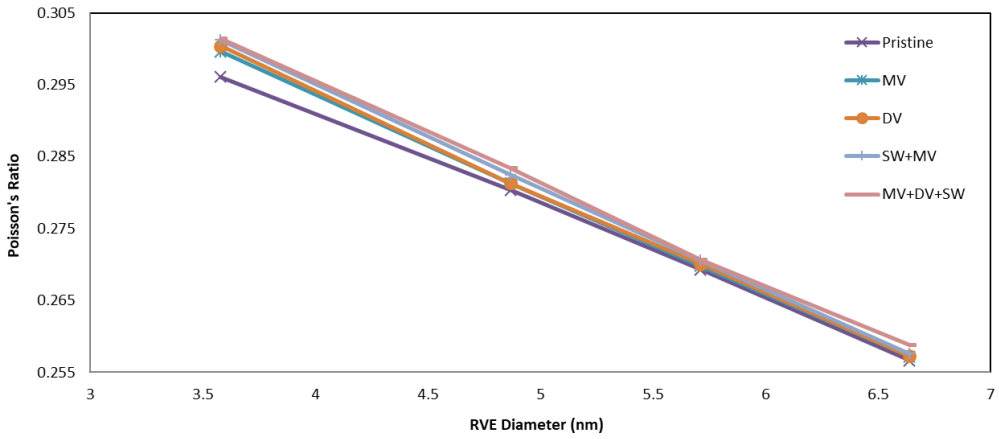

Figure 4.6 Variation of Poisson's ratio with the diameter for selected defect combinations for zigzag configuration

5. CONCLUSIONS AND FUTURE WORK

5.1. Conclusions

After the discovery of carbon nanotubes they have become a focal topic in material science and various engineering fields due to their extraordinary mechanical properties. Moreover, the properties such as high strength to weight ratio, high stiffness, high aspect ratio that they possess make them great reinforcement materials for composites. Also, usage of carbon reinforced polymer composites (CNTRPs) provide great opportunities to replace conventional materials. Moreover, in terms of environmental aspects and sustainable development, CNTRPs are very advantageous alternatives. Therefore, with all these advantageous and wide range potential application areas make CNTRPs valuable for the future. However, knowledge on the CNTRPs are not advanced and studies are still premature in this area. This thesis study aims to investigate CNTRPs with SWNTs against different randomly occurring defects on SWNTs, different chiralities, and diameters for the selected mechanical properties like Young's modulus, shear modulus, and Poisson's ratio. This thesis study is mainly divided into two parts. Investigation of defective SWNT structures for different diameters and different type of defects is the first part of the study.

In the first part, via equivalent continuum mechanics method SWNTs are developed. Investigations are conducted for a better understanding of the mechanical properties. Simulations are done by mainly axial displacement for

Young's modulus and Poisson's ratio. It can be concluded that for the Young's modulus, both zigzag and armchair configurations give similar response. For both configurations, effects of defects are much more critical in small diameters. Also, increase in defect concentration and defect type has similar effect on the tubes. Poisson's ratio is also investigated against chirality and defect types. Furthermore, shear modulus is also studied under torsional loading. Results for all Young's modulus, shear modulus, and Poisson's ratio via the proposed model are compared with similar studies in literature and mainly good agreement is seen with the literature. Thus, suggested model and the continuum equivalent method prove that it can be a useful tool to investigate mechanical properties for SWNTs with defects.

The second part of the thesis is aimed to investigate CNTRPs for predicting Young's modulus and Poisson's ratio. Epoxy resin/defective SWNT composites are modelled with the data found in the first part. For the models, perfect bonding representative volume element method is applied and fraction of volume is taken as 5% for the SWNTs. The study is conducted with axial displacement method. Beside the literature comparison, models are also validated by the analytical rule of mixtures. It can be concluded that chirality effects are critical for Young's modulus values. For zigzag configuration, decrease of Young's modulus in small dimeter SWNTs are critical and defects are not that critical in this drop. On the other hand, for the armchair configuration effect of defects are significant in small

diameters. Moreover, both Poisson's ratio and Young's modulus results are found to be comparable to works in literature and the analytical rule of mixtures.

As a result, presence of defects on lattice structure of SWNTs can be critical for the mechanical properties. The study indicates that different type of defects have different effects on properties. However, defect concentration is the most effective parameter for the selected mechanical properties. Moreover, it can be seen that size and chirality are also important factors to investigate the properties. Especially, small diameter tubes are the most vulnerable structures in case of randomly occurring defects. Although presence of defects can affect the mechanical properties for CNTRPs negatively, the values are still promising and satisfying for many future applications. Besides, in terms of cost effectiveness defective and pristine CNTs analysed. As it is noted CNT synthesis is energy intensive process. Comparison of main techniques in terms of energy requirements show that there are almost ten times difference between techniques arc discharge and CVD. In general, low temperature synthesis like CVD is the main reason of defects especially SW defects. On the other hand, high energy intensive techniques like arc discharge and laser ablation give better quality CNTs. Considering the total energy requirement percent difference between CVD and laser ablation is around 88.8% and this value is 163.9 % for arc discharge. However, drop in Young's modulus for armchair case with SW defective CNTRPs is 2.6% in average. In highest concentration this difference is 5.4%, in

average. Therefore, in terms of cost and sustainability aspects usage of CVD technique can be better solution to synthesize CNTs.

5.2. Future Work

The present study mainly focuses on three type defects which are Stone-Wales, mono and di-vacancies. Although these are the most common defects on SWNTs, there are other defects as well such as adatoms. Moreover, defect positions and concentrations can be studied in depth for a better understanding. Scope of this thesis is to delve into some of the selected mechanical properties which are Young's modulus, Poisson's ratio, and shear modulus. However, mechanical properties are not limited to those three properties. Understanding on other mechanical properties like ultimate tensile strength, rupture strength, yield strength etc. should also be improved through investigation of the defective SWNTs. Apart from these, study can be extended via addition of other chirality and diameter values. Moreover, in the present study length of tubes are kept constant and it is not considered as a critical parameter. However, investigations can be done by taking tube length as a parameter.

CNTRP analysis in the present study is only done for 5% volume fraction. As a future study varying fractions of SWNT in the polymer matrix can be investigated. Although there are many studies in literature done in nano-scale, there is a gap in

macro level modelling for the CNTRPs. Modelling and investigation macro level CNTRPs can be another area of investigation for the future work.

REFERENCES

[1] V. Sharma and V. Agarwal, “Polymer composites sustainability: environmental perspective, future trends and minimization of health risk,” *2nd Int. Conf. Environ. Sci. Dev.*, vol. 4, pp. 259–261, 2011.

[2] O. Breuer and U. Sundararaj, “Big returns from small fibers: A review of polymer/carbon nanotube composites,” *Polym. Compos.*, vol. 25, no. 6, pp. 630–645, 2004.

[3] S. Iijima, “Helical microtubules of graphitic carbon,” vol. 354, no. November, pp. 56–58, 1991.

[4] A. K.-T. Lau and D. Hui, “The revolutionary creation of new advanced materials—carbon nanotube composites,” *Compos. Part B Eng.*, vol. 33, no. 4, pp. 263–277, 2002.

[5] P. G. Collins, “Defects and Disorder in Carbon Nanotubes,” *Oxford Handb. Nanosci. Technol. Front. Adv.*, pp. 1–73, 2009.

[6] Q. Lu and B. Bhattacharya, “Effect of randomly occurring Stone-Wales defects on mechanical properties of carbon nanotubes using atomistic simulation,” *Nanotechnology*, vol. 16, no. 4, pp. 555–566, 2005.

[7] R. S. Ruoff, D. Qian, and W. K. Liu, “Mechanical properties of carbon nanotubes: Theoretical predictions and experimental measurements,” *Comptes Rendus Phys.*, vol. 4, no. 9, pp. 993–1008, 2003.

[8] R. Rafiee and R. M. Moghadam, “On the modeling of carbon nanotubes: A critical review,” *Compos. Part B Eng.*, vol. 56, pp. 435–449, 2014.

[9] T. Belin and F. Epron, “Characterization methods of carbon nanotubes: A review,” *Mater. Sci. Eng. B Solid-State Mater. Adv. Technol.*, vol. 119, no. 2, pp. 105–118, 2005.

[10] M. Rahmandoust and A. Öchsner, “On Finite Element Modeling of Single- and Multi-Walled Carbon Nanotubes,” *J. Nanosci. Nanotechnol.*, vol. 12, no. 10, pp. 8129–8136, 2012.

[11] D. Srivastava, C. Wei, and K. Cho, “Nanomechanics of carbon nanotubes and composites,” *Appl. Mech. Rev.*, vol. 56, no. 2, p. 215, 2003.

[12] M. Brcic, M. Canadija, J. Brnic, D. Lanc, S. Krscanski, and G. Vukelic, “FE modelling of multi-walled carbon nanotubes,” *Est. J. Eng.*, vol. 15, no. 2, pp. 77–86, 2009.

[13] E. Ganesh, “Single Walled and Multi Walled Carbon Nanotube Structure, Synthesis and Applications,” *Ijitee*, vol. 2, no. 4, pp. 311–320, 2013.

[14] P. Henrique, C. Camargo, K. G. Satyanarayana, and F. Wypych, “Nanocomposites_Synthesis,structure,properties and new application opportunities.pdf,” vol. 12, no. 1, pp. 1–39, 2009.

[15] P. Joshi and S. H. Upadhyay, “Evaluation of elastic properties of multi walled carbon nanotube reinforced composite,” *Comput. Mater. Sci.*, vol. 81, pp. 332–338, 2014.

[16] J. H. Du, J. Bai, and H. M. Cheng, “The present status and key problems of carbon nanotube based polymer composites,” *Express Polym. Lett.*, vol. 1, no. 5, pp. 253–273, 2007.

[17] S. O’Donnell, “Potential Impact of Carbon Nanotube Reinforced Polymer Composite on Commercial Aircraft Performance and Economics,” *Am. Inst. Aeronaut. Astronaut.*, pp. 1–10, 2004.

[18] D. Kushnir and B. A. Sandén, “Energy requirements of carbon nanoparticle production,” *J. Ind. Ecol.*, vol. 12, no. 3, pp. 360–375, 2008.

[19] C. Zhuo, “On the Synthesis of Carbon Nanotubes from Waste Solid Hydrocarbons,” 2014.

[20] J. Zuberi, “Computational Modelling of Carbon Nanotube Reinforced Polymer Composites,” 2014.

[21] Y. T. Ong, A. L. Ahmad, S. Hussein, S. Zein, and S. H. Tan, “A review on carbon nanotubes in an environmental protection and gree engineering perspective.,” *Brazilian J Chem Engi*, vol. 27, no. 02, pp. 227–242, 2010.

[22] X. Lu and Z. Hu, “Mechanical property evaluation of single-walled carbon nanotubes by finite element modeling,” *Compos. Part B Eng.*, vol. 43, no. 4, pp. 1902–1913, 2012.

[23] A. Krishnan, E. Dujardin, and T. Ebbesen, “Young’s modulus of single-walled nanotubes,” *Phys. Rev. B - Condens. Matter Mater. Phys.*, vol. 58, no. 20, pp. 14013–14019, 1998.

[24] E. Hernández, C. Goze, P. Bernier, and A. Rubio, “Elastic Properties of C and BxCyNyComposite Nanotubes,” *Phys. Rev. Lett.*, vol. 80, no. 20, pp. 4502–4505, 1998.

[25] D. Sanchez-Portal, E. Artacho, and J. M. Soler, “Ab initio structural, elastic, and vibrational properties of carbon nanotubes,” *Phys. Rev. B*, vol. 59, no. 19, pp. 12678–12688, 1999.

[26] T. Ozaki, Y. Iwasa, and T. Mitani, “Stiffness of single-walled carbon nanotubes under large strain,” *Phys. Rev. Lett.*, vol. 84, no. 8, pp. 1712–1715, 2000.

[27] M. M. Shokrieh and R. Rafiee, “On the tensile behavior of an embedded carbon nanotube in polymer matrix with non-bonded interphase region,” *Compos. Struct.*, vol. 92, no. 3, pp. 647–652, 2010.

[28] C. Li and T. W. Chou, “A structural mechanics approach for the analysis of carbon nanotubes,” *Int. J. Solids Struct.*, vol. 40, no. 10, pp. 2487–2499, 2003.

[29] K. I. Tserpes and P. Papanikos, “Finite element modeling of carbon nanotubes,” *Int. J. Mech. Mech. Eng.*, vol. 10, no. 3, pp. 19–24, 2010.

[30] J. R. Xiao, B. A. Gama, and J. W. Gillespie, “An analytical molecular structural mechanics model for the mechanical properties of carbon nanotubes,” *Int. J. Solids Struct.*, vol. 42, no. 11–12, pp. 3075–3092, 2005.

[31] M. Mahboob and M. Z. Islam, “Effect of vacancy and stone-wales defects on the shear strength of carbon nanotube-polymer interfaces,” *Adv. Mater. Res.*, vol. 970, no. i, pp. 263–266, 2014.

[32] Y. Fan, B. R. Goldsmith, and P. G. Collins, “Identifying and counting point defects in carbon nanotubes.,” *Nat. Mater.*, vol. 4, no. 12, pp. 906–911, 2005.

[33] H. Y. He and B. C. Pan, “Studies on structural defects in carbon nanotubes,” *Front. Phys. China*, vol. 4, no. 3, pp. 297–306, 2009.

[34] K. Sharma, K. K. Saxena, and M. Shukla, “Effect of multiple stone-wales and vacancy defects on the mechanical behavior of carbon nanotubes using molecular dynamics,” *Procedia Eng.*, vol. 38, pp. 3373–3380, 2012.

[35] N. A. Sakharova, A. F. G. Pereira, J. M. Antunes, and J. V. Fernandes, “Numerical simulation study of the elastic properties of single-walled carbon nanotubes containing vacancy defects,” *Compos. Part B Eng.*, vol. 89, pp. 155–168, 2016.

[36] A.A. Rashad, R. Noaman, S. A. Mohammed, and E. Yousif, “Synthesis of carbon nanotube: A review,” vol. 2, no. 3, pp. 3–4, 2014.

[37] K. Awasthi, A. Srivastava, and O. N. Srivastava, “Synthesis of Carbon Nanotubes,” vol. 5, no. 10, pp. 1–65, 2005.

[38] A. Szabó, C. Perri, A. Csató, G. Giordano, D. Vuono, and J. B. Nagy, “Synthesis methods of carbon nanotubes and related materials,” *Materials (Basel).*, vol. 3, no. 5, pp. 3092–3140, 2010.

[39] A. Jorio, G. Dresselhaus, and M. S. Dresselhaus, *Topics in Applied Physics Volume 111. Carbon Nanotubes*, vol. 111. 2008.

[40] M. R. Ayatollahi, S. Shadlou, and M. M. Shokrieh, “Multiscale modeling for mechanical properties of carbon nanotube reinforced nanocomposites subjected to different types of loading,” *Compos. Struct.*, vol. 93, no. 9, pp. 2250–2259, 2011.

[41] R. Rafiee, A. Fereidoon, and M. Heidarhaei, “Influence of non-bonded interphase on crack driving force in carbon nanotube reinforced polymer,” *Comput. Mater. Sci.*, vol. 56, pp. 25–28, 2012.

[42] R. Rafiee and R. Maleki Moghadam, “Simulation of impact and post-impact behavior of carbon nanotube reinforced polymer using multi-scale finite element modeling,” *Comput. Mater. Sci.*, vol. 63, pp. 261–268, 2012.

[43] A. K. Gupta and S. P. Harsha, “Analysis of mechanical properties of carbon nanotube reinforced polymer composites using multi-scale finite element modeling approach,” *Compos. Part B Eng.*, vol. 95, no. Icmpc, pp. 172–178, 2016.

[44] F. Scarpa and S. Adhikari, “A mechanical equivalence for Poisson’s ratio and

thickness of C-C bonds in single wall carbon nanotubes," *J. Phys. D. Appl. Phys.*, vol. 41, no. 8, pp. 7–12, 2008.

[45] M. Jibran, S. Zuberi, and V. Esat, "ESDA2014-20156 ESTIMATING THE EFFECT OF CHIRALITY AND SIZE ON THE MECHANICAL PROPERTIES OF CARBON NANOTUBES THROUGH FINITE ELEMENT," pp. 1–7, 2016.

[46] F. Karimzadeh, S. Ziaei-Rad, and S. Adibi, "Modeling considerations and material properties evaluation in analysis of carbon nano-tubes composite," *Metall. Mater. Trans. B Process Metall. Mater. Process. Sci.*, vol. 38, no. 4, pp. 695–705, 2007.

[47] B. I. Yakobson, C. J. Brabec, and J. Bernholc, "Nanomechanics of carbon tubes: Instabilities beyond linear response," *Phys. Rev. Lett.*, vol. 76, no. 14, pp. 2511–2514, 1996.

[48] G. M. Odegard, T. S. Gates, L. M. Nicholson, and K. E. Wise, "Equivalent-continuum modeling of nano-structured materials," *Compos. Sci. Technol.*, vol. 62, no. 14, pp. 1869–1880, 2002.

[49] M. J. S. Zuberi and V. Esat, "Evaluating the effects of size and chirality on the mechanical properties of single-walled carbon nanotubes through equivalent-continuum modelling," *Proc. Inst. Mech. Eng. Part L J. Mater. Des. Appl.*, vol. 230, no. 5, pp. 913–926, 2016.

[50] M. Meo and M. Rossi, "Prediction of Young ' s modulus of single wall carbon nanotubes by molecular-mechanics based finite element modelling," *Compos. Sci. Technol.*, vol. 66, pp. 1597–1605, 2006.

[51] A. F. Ávila and G. S. R. Lacerda, "Molecular mechanics applied to single-walled carbon nanotubes," *Mater. Res.*, vol. 11, no. 3, pp. 325–333, 2009.

[52] L. Chen, Q. Zhao, Z. Gong, and H. Zhang, "The effects of different defects on the elastic constants of single-walled carbon nanotubes," *2010 IEEE 5th Int. Conf. Nano/Micro Eng. Mol. Syst. NEMS 2010*, no. 50605039, pp. 777–780, 2010.

[53] J. M. Wernik and S. A. Meguid, "Multiscale modeling of the nonlinear response of nano-reinforced polymers," *Acta Mech.*, vol. 217, no. 1–2, pp. 1–16, 2011.

[54] M. J. S. Zuberi and V. Esat, "Investigating the mechanical properties of single walled carbon nanotube reinforced epoxy composite through finite element modelling," *Compos. Part B Eng.*, vol. 71, pp. 1–9, 2015.

[55] J. N. Coleman, U. Khan, W. J. Blau, and Y. K. Gun'ko, "Small but strong: A review of the mechanical properties of carbon nanotube-polymer composites," *Carbon N. Y.*, vol. 44, no. 9, pp. 1624–1652, 2006.

APPENDICES

Appendix A: Characteristics of FE models for SWNT and CNTRPs

Table A. 1 FE model data for pristine zigzag configuration SWNTs

Configuration	L_{CNT} (nm)	D_{CNT} (nm)	# Nodes	# Elements
(6,0)	12.354	0.470	696	1032
(11,0)	11.928	0.861	1232	1837
(15,0)	12.354	1.174	1740	2595
(20,0)	12.354	1.565	2320	3440
(25,0)	12.354	1.956	2900	4299

Table A. 2 FE model data for pristine armchair configuration SWNTs

Configuration	L_{CNT} (nm)	D_{CNT} (nm)	# Nodes	# Elements
(6,6)	12.052	0.814	1176	1752
(10,10)	12.052	1.355	1960	2920
(12,12)	12.052	1.628	2352	3504
(15,15)	12.052	2.035	2940	4380
(20,20)	12.054	2.700	3960	5900

Table A. 3 FE model data for pristine zigzag configuration CNTRPs

Configuration	$R_{Interphase}$ (nm)	R_{CNTRP} (nm)	L_{CNTRP} (nm)	# Nodes	# Elements
(6,0)	0.470	1.789	7.377	7440	6600
(11,0)	0.861	2.434	7.377	8680	7800
(15,0)	1.174	2.856	7.377	9300	8400
(20,0)	1.566	3.320	7.377	10540	9600

Table A. 4 FE model data for pristine armchair configuration CNTRPs

Configuration	$R_{Interphase}$ (nm)	R_{CNTRP} (nm)	L_{CNTRP} (nm)	# Nodes	# Elements
(3,3)	0.407	1.664	7.377	6820	6000
(6,6)	0.814	2.365	7.377	8060	7200
(10,10)	1.356	3.076	7.377	9920	9000
(12,12)	1.627	3.388	7.377	10540	9600

Appendix B: Simulation Results for Chapter 3 & 4

Table B. 1 Simulation results for armchair (6,6)

Defects	ΔL (nm)	E (TPa)	ν	Torsional load (Nm nm)	G (TPa)
Pristine	0.1	0.887	0.279	1.200	0.300
MV	0.1	0.879	0.507	1.200	0.211
DV	0.1	0.877	0.531	1.200	0.197
SW	0.1	0.860	0.288	1.200	0.221
MV+SW	0.1	0.853	0.744	1.200	0.198
MV+DV+SW	0.1	0.850	0.949	1.200	0.197

Table B. 2 Simulation results for armchair (10,10)

Defects	ΔL (nm)	E (TPa)	ν	Torsional load (Nm nm)	G (TPa)
Pristine	0.1	0.888	0.254	2.000	0.347
MV	0.1	0.885	0.480	2.000	0.298
DV	0.1	0.883	0.408	2.000	0.275
SW	0.1	0.874	0.285	2.000	0.274
MV+SW	0.1	0.870	0.451	2.000	0.269
MV+DV+SW	0.1	0.858	0.775	2.000	0.258

Table B. 3 Simulation results for armchair (12,12)

Defects	ΔL (nm)	E (TPa)	ν	Torsional load (Nm nm)	G (TPa)
Pristine	0.1	0.887	0.250	2.400	0.349
MV	0.1	0.884	0.349	2.400	0.306
DV	0.1	0.884	0.390	2.400	0.295
SW	0.1	0.875	0.305	2.400	0.283
MV+SW	0.1	0.871	0.415	2.400	0.276
MV+DV+SW	0.1	0.862	0.613	2.400	0.276

Table B. 4 Simulation results for armchair (15,15)

Defects	ΔL (nm)	E (TPa)	ν	Torsional load (Nm nm)	G (TPa)
Pristine	0.1	0.887	0.244	3.000	0.364
MV	0.1	0.885	0.299	3.000	0.304
DV	0.1	0.885	0.316	3.000	0.296
SW	0.1	0.874	0.301	3.000	0.291
MV+SW	0.1	0.872	0.376	3.000	0.288
MV+DV+SW	0.1	0.864	0.524	3.000	0.287

Table B. 5 Simulation results for armchair (20,20)

Defects	ΔL (nm)	E (TPa)	ν
Pristine	0.1	0.889	0.186
MV	0.1	0.888	0.256
DV	0.1	0.887	0.212
SW	0.1	0.878	0.213
MV+SW	0.1	0.876	0.243
MV+DV+SW	0.1	0.870	0.284

Table B. 6 Simulation results for zigzag (6,0)

Defects	ΔL (nm)	E (TPa)	ν	Torsional load (Nm nm)	G (TPa)
Pristine	0.1	0.809	0.296	0.600	0.269
MV	0.1	0.794	0.526	0.600	0.236
DV	0.1	0.788	0.547	0.600	0.211
SW	0.1	0.802	0.413	0.600	0.209
MV+SW	0.1	0.786	0.565	0.600	0.201
MV+DV+SW	0.1	0.767	0.591	0.600	0.195

Table B. 7 Simulation results for zigzag (11,0)

Defects	ΔL (nm)	E (TPa)	ν	Torsional load (Nm nm)	G (TPa)
Pristine	0.1	0.866	0.245	1.100	0.315
MV	0.1	0.859	0.399	1.100	0.269
DV	0.1	0.857	0.401	1.100	0.260
SW	0.1	0.852	0.364	1.100	0.256
MV+SW	0.1	0.845	0.417	1.100	0.252
MV+DV+SW	0.1	0.836	0.466	1.100	0.248

Table B. 8 Simulation results for zigzag (15,0)

Defects	ΔL (nm)	E (TPa)	ν	Torsional load (Nm nm)	G (TPa)
Pristine	0.1	0.878	0.234	1.500	0.339
MV	0.1	0.873	0.363	1.500	0.291
DV	0.1	0.871	0.374	1.500	0.288
SW	0.1	0.861	0.352	1.500	0.281
MV+SW	0.1	0.856	0.375	1.500	0.278
MV+DV+SW	0.1	0.850	0.338	1.500	0.274

Table B. 9 Simulation results for zigzag (20,0)

Defects	ΔL (nm)	E (TPa)	ν	Torsional load (Nm nm)	G (TPa)
Pristine	0.1	0.882	0.229	2.000	0.339
MV	0.1	0.878	0.336	2.000	0.306
DV	0.1	0.877	0.335	2.000	0.297
SW	0.1	0.874	0.322	2.000	0.295
MV+SW	0.1	0.870	0.354	2.000	0.291
MV+DV+SW	0.1	0.864	0.369	2.000	0.290

Table B. 10 Simulation results for zigzag (25,0)

Defects	ΔL (nm)	E (TPa)	ν	Torsional load (Nm nm)	G (TPa)
Pristine	0.1	0.884	0.230	2.500	0.345
MV	0.1	0.881	0.325	2.500	0.312
DV	0.1	0.880	0.314	2.500	0.309
SW	0.1	0.880	0.315	2.500	0.311
MV+SW	0.1	0.877	0.330	2.500	0.308
MV+DV+SW	0.1	0.874	0.358	2.500	0.305

Table B. 11 Simulation results for armchair CNTRP configuration

	Pristine	**MV**	**DV**	**SW**	**MV+SW**	**MV+DV+SW**
	E (GPa)	**E (GPa)**	**E (GPa)**	**E (GPa)**	**E (GPa)**	**E (GPa)**
(3,3)	53.712	52.714	52.434	50.678	49.371	47.657
(6,6)	54.160	53.784	53.665	52.837	52.485	51.356
(10,10)	54.803	54.607	54.577	54.156	53.953	53.355
(12,12)	55.076	54.898	54.879	54.429	54.261	53.782

Table B. 12 Simulation results for zigzag CNTRP configuration

	Pristine	**MV**	**DV**	**SW**	**MV+SW**	**MV+DV+SW**
	E (GPa)	**E (GPa)**	**E (GPa)**	**E (GPa)**	**E (GPa)**	**E (GPa)**
(6,0)	49.659	48.898	48.597	49.293	48.478	47.579
(11,0)	53.045	52.680	52.566	52.334	51.974	51.549
(15,0)	53.953	53.706	53.637	53.139	52.897	52.566
(20,0)	54.645	54.467	54.384	54.231	54.048	53.816